The Analysis of Inflatable Antennas Using A Corotational Finite Element Approach

(Interim Report)

A. N. Palazotto, Principal Investigator
J. O. Choi, Research Associate

DEPARTMENT OF THE AIR FORCE
AIR UNIVERSITY
AIR FORCE INSTITUTE OF TECHNOLOGY

Wright-Patterson Air Force Base, Ohio

19980925 001

AFIT/ENY/TR-98-04

The Analysis of Inflatable Antennas Using A Corotational Finite Element Approach

(Interim Report)

A. N. Palazotto, Principal Investigator
J. O. Choi, Research Associate

AFIT/ENY/TR-98-02

Approved for public release; distribution unlimited

AFIT/ENY/TR-98-04

The Analysis of Inflatable Antennas Using A Corotational Finite Element Approach

Prepared by

A. N. Palazotto, Principal Investigator
J. O. Choi, Research Associate

(Interim Report)

Approved for public release; distribution unlimited

Department of Aeronautics and Astronautics
Air Force Institute of Technology
WPAFB, OH 45433

The views expressed in this report are those of the authors and do not reflect the official policy or position of the Department of Defense or the U.S. Government

Abstract

The Jaumann stress-strain approach has been used to evaluate a nonlinear structural response to a shell like geometry. The method employs a finite element solution incorporating the Jaumann stress-strain relationships based on large displacement and large rotation using a corotational technique. The resulting equations include the continuity of stresses and displacements in the thickness direction. Thus, it is possible to evaluate the effects of direct and shear stresses within a laminated structure.

Initial comparisons of the method of analysis has been made with two other theories. The first is the total Lagrangian theory based on an in-house program, and the second is an Eulerian based theory defined by ABAQUS. Several problems have been attempted including a cylindrical shell panel made from composite materials undergoing nonlinear collapse. Two new algorithm have been developed; the first to consider a nonconservative force system and the second to transform the resulting equations from a curvilinear coordinate system into a Cartesian system. The last algorithm defines a global set of equations which can be used for the mixture of various element geometries.

Results show that the need for a correct through the thickness evaluation of the stresses of the shell is required as the shell thickness increases relative to the resulting geometry. In a predominantly membrane resistant structure, the three types of theories, Eulerian, Jaumann and Lagrangian show close comparison.

Acknowledgement

The author gratefully acknowledge the sponsorship of J. A . Bishop, Space System development Engineer, Air Force Research Laboratory Kirtland AFB, NM.

Contents

List of Tables

List of Figures

1 Introduction

The focus of this research is to carry out an analysis of satellite antennas made from various composite materials incorporating a program which can be specifically directed toward this type of structure without resorting to commercial programs. In this inflatable structure, a paraboloidal shape is desired for optical and RF(Radio Frequency) reflectors [1][4][5] because of their scientific use. Thus, the major concern is to obtain a membrane space structure which approaches a paraboloid geometry under internal pressure. Therefore, this research is an attempt at developing a robust but efficient finite element program which can simulate the major characteristics of the need for arriving at an approximate final geometry. The method employed is one which incorporates the concept of large movement due to a nonconservative pressure loading (one that remains normal to the deforming structure). This method is based upon the Jaumann stress-strain relationships using the corotational[2][3] technique. The resulting equations include the continuity of stresses and displacements in the thickness direction. Thus, it is possible to evaluate the effects of direct and shear stresses within a laminated structure and trace any nonlinear geometric characteristics.

In this first report, the Jaumann relations are developed within a total

Lagrangian system using a corotational approach. An in-house computer program(JAGS[1]) is modified to handle the appropriate geometries and results are compare to an Eulerian based program, ABAQUS. Several problems have been attempted including; a cylindrical shell panel made from composite materials undergoing nonlinear collapse; an isotropic membrane acted upon by a nonconservative force system and a parabolic shell acted upon by a pressure loading. These problems verify the accuracy of the theory and program.

Results show that the need for a correct through the thickness evaluation of the stresses of the shell is required as the shell thickness increases relative to the resulting geometry. In predominantly membrane resistant structures the comparison among the three types of theories, Eulerian, Jaumann and Lagrangian(SLR[2][6], LDLR[3][7]) are very close.

2 Theory

In this section, a brief review of the corotation theory leading to the Jaumann stress-strain relationship is carry out. This theory is presented to show a total

[1] Jaumann Analysis of General Shells

[2] Simplified Large Displacement and Moderately Large Rotation

[3] Large Displacement and Large Rotation

Lagrangian corotational approach. Much of this development can be found in several papers written by Palazotto et. al.[7] - [10].

2.1 A Total Lagrangian Corotational Finite Element Scheme used in the Analysis of An Inflatable Shell

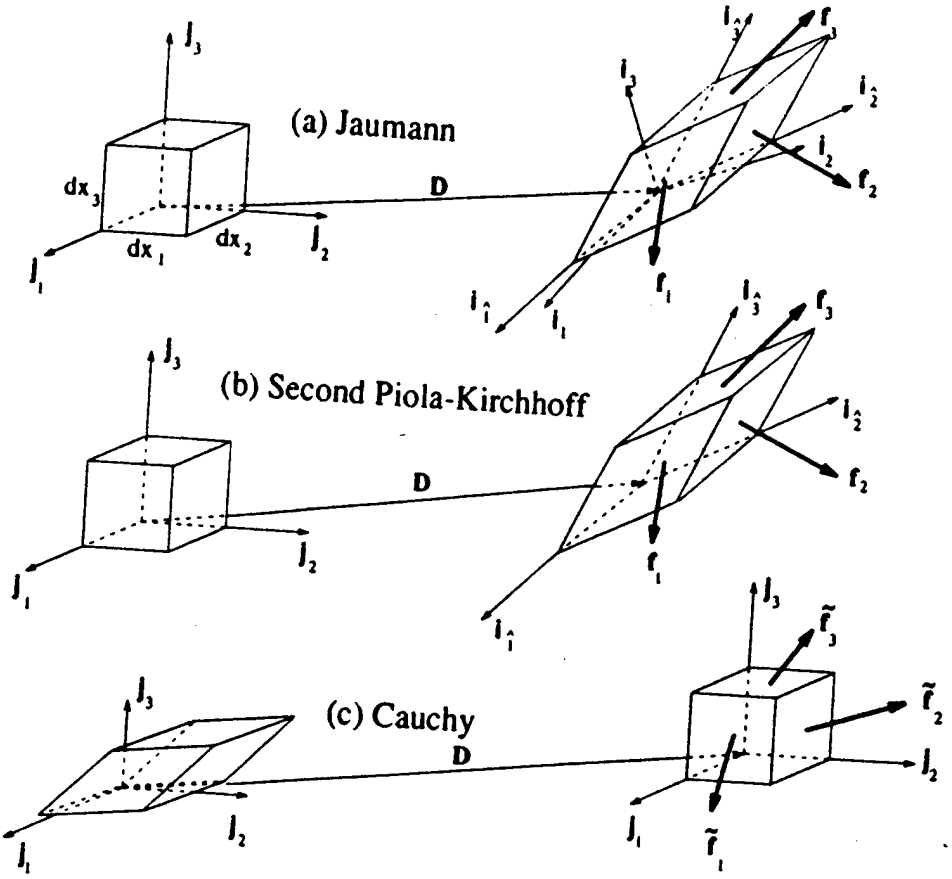

Figure 1: Deformation of an infinitesimal volumn element.

The theory makes use of the polar decomposition method to facilitate the use of a local (and linear) displacement field at an infinitesimal region of interest in the nonlinear deforming body. The Jaumann stress[11] J_{mn} and strain B_{mn} are given by

$$J_{mn} = \frac{1}{2\,dx_1\,dx_2\,dx_3}\left(dx_m\,\mathbf{f}_m \cdot \mathbf{i}_n + dx_n\,\mathbf{f}_m \cdot \mathbf{i}_m\right) \tag{1}$$

$$B_{mn} = \frac{1}{2}\left(\frac{\partial \mathbf{u}}{\partial x^m} \cdot \mathbf{i}_n + \frac{\partial \mathbf{u}}{\partial x^n} \cdot \mathbf{i}_m\right) \tag{2}$$

where the $\mathbf{f}_m$ are the force resultants on the faces of the deformed parallelepiped (Figure 1). For example, $\mathbf{f}_1$ acts on the deformed $dx_2 - dx_3$ plane. The local displacement vector $\mathbf{u}$ of equation(2) is measured with respect to the displaced location of a material point, hence at any given point on the deformed reference surface, $\mathbf{u} = 0$, though its derivatives (which will give rise to the strains) are non-zero. The Jaumann stresses and strains are defined with respect to the orthogonal directions, denoted by unit vectors $\mathbf{i}_k$, associated with the stretched and rigidly rotated volume element (Figure 1(a)). On the other hand, the second Piola-Kirchhoff stresses S_{mn} and Green's strain L_{mn} are defined by

$$\frac{1}{dx_1\,dx_2\,dx_3} dx_{(m)}\,\mathbf{f}_{(m)} = \sum_{n=1}^{3}\left(S_{m(n)}\,\lambda_n\,\hat{\mathbf{i}}_{(n)}\right) \tag{3}$$

$$L_{mn} = \frac{1}{2}\left(\lambda_m \mathbf{i}_{(\widehat{m})} \cdot \lambda_n \mathbf{i}_{(\widehat{n})}\right) \tag{4}$$

where λ_n is the magnitude of so-called "lattice vector", and the parentheses suspend the tensor summing convention. In the figure, it is seen that the Second - Piola/Green measures are associated with the directions along the deformed (and, in general, not orthogonal) edges of the element, as shown in Figure 1(b). The directions of the lattice vector correspond to the directions of the unit vectors $\mathbf{i}_{\widehat{k}}$. So, in general, the component of the Second Piola stresses are along neither those of the undeformed coordinate system, as are the Eulerian measures depicted in Figure 1(c), nor those of its rigidly translated and rotated counterpart in the deformed body (as are the Jaumann measures). This is a consequence of the Green strains being energy related measures rather than strictly geometric measures, like Jaumann or engineering strains. To use the Jaumann measures, which are local, the effect of rigid body translation and rotation must be removed so that the effect of stretching is seen.

In a layered composite consisting of N layers, the local displacement vector with respect to the local $\xi\eta\zeta$ coordinate system of Fig.(2) as presented in Pai and Palazotto[3] is defined as

$$\mathbf{u} = u_1^{(i)}\mathbf{i}_1 + u_2^{(i)}\mathbf{i}_2 + u_3^{(i)}\mathbf{i}_3 \tag{5}$$

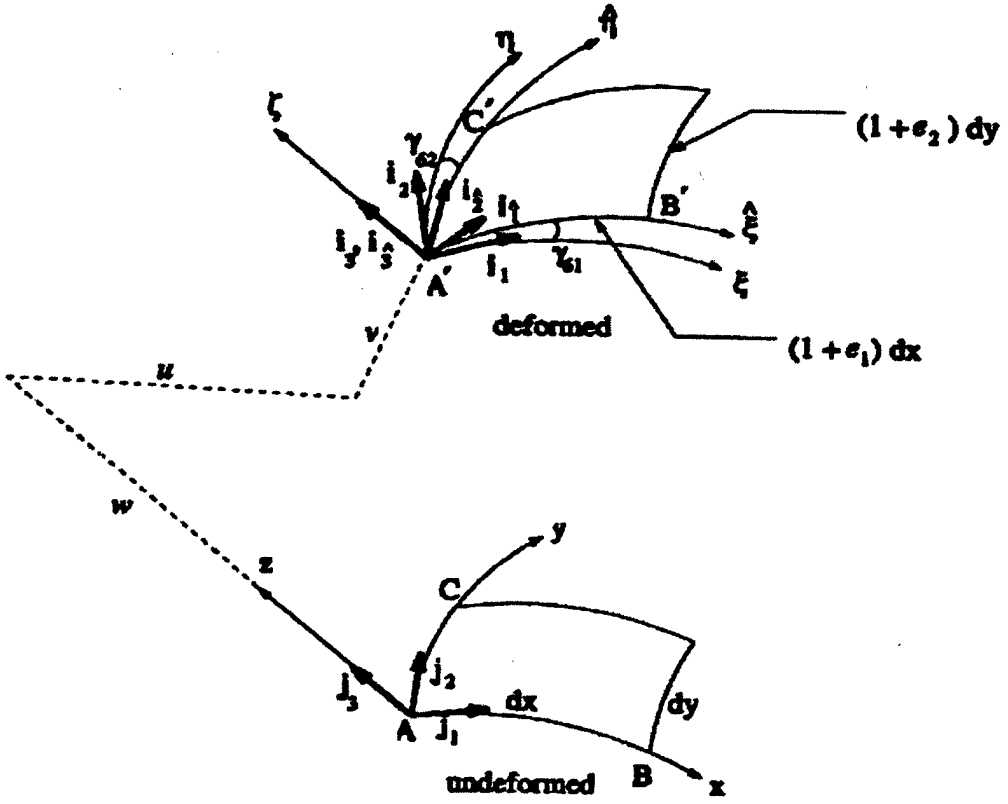

Figure 2: Infinitesimal element undergoing deformation(after Pai and Palazotto, 1995)

where

$$
\begin{aligned}
u_1^{(i)} &= u_1^0(x,y) + z\left[\theta_2(x,y) - \theta_2^0(x,y)\right] + \gamma_5 z + \alpha_1^{(i)}(x,y)\, z^2 + \beta_1^{(i)}(x,y)\, z^3 \\
u_2^{(i)} &= u_2^0(x,y) + z\left[\theta_1(x,y) - \theta_1^0(x,y)\right] + \gamma_4 z + \alpha_2^{(i)}(x,y)\, z^2 + \beta_2^{(i)}(x,y)\, z^3 \\
u_3^{(i)} &= u_3^0(x,y) + \alpha_3^{(i)}(x,y)\, z + \beta_3^{(i)}(x,y)\, z^2
\end{aligned}
$$

Here, u_j^0 $(j = 1, 2, 3)$ are the components of displacement (with respect to the local coordinate system $\xi\eta\zeta$) of a point which is located on the reference surface at (x, y) before deformation. The rigid body rotations and shear rotations are given by θ and γ, respectively. The angle between the transverse coordinate z and the normal to the reference surface in the undeformed configuration as measured in the xz plane is given by θ_1^0. The corresponding angle in the yz plane is given by θ_2^0. The shear rotation angle in the xz plane at the reference surface is denoted by γ_5, and represents the rotation of the normal to the reference surface due to transverse shear deformation. The corresponding angle in the yz plane is γ_4. The terms $\alpha_k^{(i)}$ and $\beta_k^{(i)}$, are referred to as shear warping and thickness stretch functions. These functions are used to describe the kinematic behavior, beyond simple rotation of the rigid normal, of the material away from the reference surface, and allow coupling of the displacement $u_1^{(i)}$ and $u_2^{(i)}$ via the shear angles at the reference surface.

That is, γ_5 can affect displacement $u_1^{(i)}$ through the warping functions and, likewise, γ_4 can affect $u_2^{(i)}$. By defining the shear warping functions, G_1 and G_2, and the thickness stretch function, G_3 as

$$G_1 \equiv \gamma_5 z + \alpha_1^{(i)} z^2 + \beta_1^{(i)} z^3,\ G_2 \equiv \gamma_4 z + \alpha_2^{(i)} z^2 + \beta_2^{(i)} z^3 \text{ and } G_3 \equiv \alpha_3^{(i)} z + \beta_3^{(i)} z^2, \tag{6}$$

the kinematics of the eqn.(6) may be written as

$$\begin{aligned} u_1^{(i)} &= u_1^0(x,y) + z\left[\theta_2(x,y) - \theta_2^0(x,y)\right] + G_1 \\ u_2^{(i)} &= u_2^0(x,y) + z\left[\theta_1(x,y) - \theta_1^0(x,y)\right] + G_2 \\ u_3^{(i)} &= u_3^0(x,y) + G_3. \end{aligned} \tag{7}$$

The stretch function G_3 is usually small, especially for thin shells and one may neglect G_3 and its derivatives in most strain-displacement expressions. This is based upon the claim that the effect of transverse shear strain on the in-plane strain is negligible. Under this assumption, the Jaumann strain displacement relations become

$$B_{11}^{(i)} = \frac{\partial \mathbf{u}}{\partial x} \cdot \mathbf{i}_1 = (1+e_1)\cos\gamma_{61} - 1 + z\left(k_1 - k_1^0\right) + G_{1,x} - k_5 G_2 \tag{8}$$

$$B_{22}^{(i)} = \frac{\partial \mathbf{u}}{\partial y} \cdot \mathbf{i}_2 = (1+e_2)\cos\gamma_{62} - 1 + z\left(k_2 - k_2^0\right) + G_{2,y} - k_4 G_1 \tag{9}$$

$$B_{33}^{(i)} = \frac{\partial \mathbf{u}}{\partial z} \cdot \mathbf{i}_3 = 1 \tag{10}$$

$$2B_{23}^{(i)} = \frac{\partial \mathbf{u}}{\partial y} \cdot \mathbf{i}_3 + \frac{\partial \mathbf{u}}{\partial z} \cdot \mathbf{i}_2 = G_{2,z} - k_{62} G_1 - k_2 G_2 \tag{11}$$

$$2B_{13}^{(i)} = \frac{\partial \mathbf{u}}{\partial x} \cdot \mathbf{i}_3 + \frac{\partial \mathbf{u}}{\partial z} \cdot \mathbf{i}_1 = G_{1,z} - k_1 G_1 - k_{61} G_2 \tag{12}$$

$$\begin{aligned} 2B_{12}^{(i)} &= \frac{\partial \mathbf{u}}{\partial x} \cdot \mathbf{i}_2 + \frac{\partial \mathbf{u}}{\partial y} \cdot \mathbf{i}_1 \\ &= (1+e_1)\sin\gamma_{61} + (1+e_2)\sin\gamma_{62} + z\left(k_6 - k_6^0\right) \\ &\quad + G_{2,z} - k_{62} G_1 - k_2 G_2 \end{aligned} \tag{13}$$

where $k_6 = k_{61} + k_{62}$ and $k_6^0 = k_{61}^0 + k_{62}^0$.

For comparison, the total Lagrangian LDLR making use of the Green stain tensor, incorporates the kinetics, written in global Lagrangian cylindrical coordinates, as

$$\begin{aligned} u_1 &= u + z\sin(\psi_1)\cos(\psi_2) \\ u_2 &= v\left(1 - \frac{z}{R}\right) + z\sin(\psi_2) \\ u_3 &= w + z\{\cos(\psi_1)\sin(\psi_2) - 1\} \end{aligned} \tag{14}$$

where ψ_1 is the angle made by the deformed normal to the original normal in the x-z plane, and ψ_2 is the angle made by the deformed normal to the original normal in the y-z plane. The bending angles ψ_1 and ψ_2 are similar to Euler angles for rigid body motion. u, v and w are the displacements of i-th layer on the mid plane and R is the radius of the shell. This is a first order shear theory with a linear through the thickness shear, and the kinematic

assumption violates the zero shear condition on the top and bottom surfaces. Also, it can be observed that by using a small angle approximation for both ψ_1 and ψ_2, the basic kinematics used in the SLR theory is obtained. The kinematics used in the SLR theory are based on the third order shear deformation theory which assumes that the through thickness shear is a parabolic curve. This theory also makes use of the Green strain tensor but assumes relative small rotations. A detailed description regarding the derivation of the applicable kinematics that can be used for large kinematics is presented in Gummadi and Palazotto[13].

The relationship between the Jaumann stresses, J_{mn}, and the Jaumann (or Biot-Cauchy Jaumann) strains, B_{mn}, for the ith lamina of transversely isotropic material may then be written as (for the transformed relationships)

$$\begin{Bmatrix} J_{11}^{(i)} \\ J_{22}^{(i)} \\ J_{33}^{(i)} \\ J_{12}^{(i)} \\ J_{23}^{(i)} \\ J_{13}^{(i)} \end{Bmatrix} = \begin{bmatrix} \overline{Q}_{11}^{(i)} & \overline{Q}_{12}^{(i)} & \overline{Q}_{13}^{(i)} & \overline{Q}_{16}^{(i)} & 0 & 0 \\ \overline{Q}_{12}^{(i)} & \overline{Q}_{22}^{(i)} & \overline{Q}_{23}^{(i)} & \overline{Q}_{26}^{(i)} & 0 & 0 \\ \overline{Q}_{13}^{(i)} & \overline{Q}_{23}^{(i)} & \overline{Q}_{33}^{(i)} & \overline{Q}_{36}^{(i)} & 0 & 0 \\ \overline{Q}_{16}^{(i)} & \overline{Q}_{26}^{(i)} & \overline{Q}_{36}^{(i)} & \overline{Q}_{66}^{(i)} & 0 & 0 \\ 0 & 0 & 0 & 0 & \overline{Q}_{44}^{(i)} & \overline{Q}_{45}^{(i)} \\ 0 & 0 & 0 & 0 & \overline{Q}_{45}^{(i)} & \overline{Q}_{55}^{(i)} \end{bmatrix} \begin{Bmatrix} B_{11}^{(i)} \\ B_{22}^{(i)} \\ B_{33}^{(i)} \\ 2B_{12}^{(i)} \\ 2B_{23}^{(i)} \\ 2B_{13}^{(i)} \end{Bmatrix}. \quad (15)$$

The first variation of potential energy on an element basis is represented as

$$\begin{aligned}\delta\Pi &= \frac{1}{2}\sum_{i=1}^{N}\int\int\int_V \left(\delta\left[\mathbf{B}^{(i)}\right]^T \left[\overline{\mathbf{Q}}^{(i)}\right]\left[\mathbf{B}^{(i)}\right] + \left[\mathbf{B}^{(i)}\right]^T \left[\overline{\mathbf{Q}}^{(i)}\right]\delta\left[\mathbf{B}^{(i)}\right]\right) dV \\ &= \sum_{i=1}^{N}\int\int\int_V \delta\left[\mathbf{B}^{(i)}\right]^T \left[\mathbf{B}^{(i)}\right]\, dV \quad (N = number\ of\ layers) \end{aligned} \tag{16}$$

where V is the undeformed volume of the shell element structure and (i) refers to the value of the function in the ith layer of the laminate. And the $\left[\overline{\mathbf{Q}}^{(i)}\right]$ is a transformed stiffness matrix of principal stiffness matrix $\left[\mathbf{Q}^{(i)}\right]$ for the ith laminar with respect to the ξ axis, while $\left[\mathbf{B}^{(i)}\right]$ is the Jaumann strain in the ith laminar with respect to the ξ axis. Figure (3) shows a four noded 44 degree of freedom (DOF) finite element. The 11 degree of freedom at each corner are u; $u_{,x}$; $u_{,y}$; v; $v_{,x}$; $v_{,y}$; w; $w_{,x}$; $w_{,y}$; γ_4 and γ_5. Hermitian shape functions are used for all DOF except the transverse shear DOF γ_4 and γ_5, which use bilinear shape functions. In order to solve the nonlinear finite element equations, the Newton-Raphson method is used

$$\sum_{j=1}^{N_e}\left[\mathbf{K}^{[j]}\right]\left\{\Delta\mathbf{q}^{[j]}\right\} = \sum_{j=1}^{N_e}\left(\left\{\mathbf{R}^{[j]}\right\} - \left[\mathbf{K}^{[j]}\right]\left\{\mathbf{q}^{[j]}\right\}\right)_{\left\{\mathbf{q}^{[j]}\right\}=\{\mathbf{q}^0\}} \tag{17}$$

where $\left\{\mathbf{R}^{[j]}\right\}$ is the elemental nodal loading vector, $\left[\mathbf{K}^{[j]}\right]$ is so called tangent stiffness matrix, $\{\mathbf{q}^0\}$ is the displacement vector at the last converged increment. $\left\{\mathbf{q}^{[j]}\right\}$ represents the current nodal displacements, and N_e is the total number of elements making up the model. The product $\left[\mathbf{K}^{[j]}\right]\left\{\mathbf{q}^{[j]}\right\}_{\left\{\mathbf{q}^{[j]}\right\}=\{\mathbf{q}^0\}}$

is a vector described as follows,

$$\left[\mathbf{K}^{[j]}\right]\left\{\mathbf{q}^{[j]}\right\}_{\left\{\mathbf{q}^{[j]}\right\}=\left\{\mathbf{q}^{0}\right\}} = \int\int_{A^{[j]}} \underset{44\times24}{[\mathbf{D}]}^{T} \underset{24\times12}{\left[\mathbf{\Psi}^{0}\right]}^{T} \underset{12\times12}{[\mathbf{\Phi}]} \underset{12\times1}{\left\{\psi^{0}\right\}}\, dx\, dy. \qquad (18)$$

The formulation of the matrices in the above equation is described in detail in the reference of Pai and Palazotto[11] also in Greer and Palazotto[12]. Detailed explanation for the terms in equations (18) are shown in Appendix A. These terms relate to the variation of the functions of the displacement gradient. In addition $\underset{24\times12}{[\mathbf{\Psi}^{0}]}^{T}$ is a known matrix at $\{\mathbf{q}^{0}\}$.

2.2 Global Coordinates Representation of Elements Using Transformation Matrix

In order to incorporate an element developed in a local curvilinear coordinate system with other elements in their own local coordinate system, one must carry out a transformation to a global coordinate. It is appropriate to make use of a Cartesian system for this purpose. In order for this to be establish, one must evaluate a transformation based upon the appropriate orthonormal system and its direction with respect to the Cartesian axes. In this section, the authors develope the relationships between the Jaumann coordinate system, employing a local curvilinear coordinate system and the

global Cartesian coordinate system. (As yet, these expressions have not been implemented within the program)

It is possible to express the equilibrium state in the original local coordinate system using the equation

$$[K_\alpha]\{u_\alpha\} = \{R_\alpha\} \tag{19}$$

where subscript α represents local curvilinear coordinate systems.

If we were to express the same state of equilibrium in a Cartesian system, one would find

$$[K_x]\{u_x\} = \{R_x\} \tag{20}$$

where subscript x represents global Cartesian coordinate systems.

The transformation matrix $[T]$ between the local curvilinear coordinate system and global Cartesian coordinate system for an element is next introduced yielding

$$\underset{44\times1}{\{u_\alpha\}} = [T]\ \underset{44\times1}{\{u_x\}}\ . \tag{21}$$

The $[T]$ matrix is a matrix that has a rank of 44x44 if one considers a shell element as in Figure (3). Thus each degree of freedom in the Cartesian system is transformed into the appropriate degree of freedom in the curvilinear system. The $[T]$ matrix is developed as following; The vector $\overline{A}$ can be

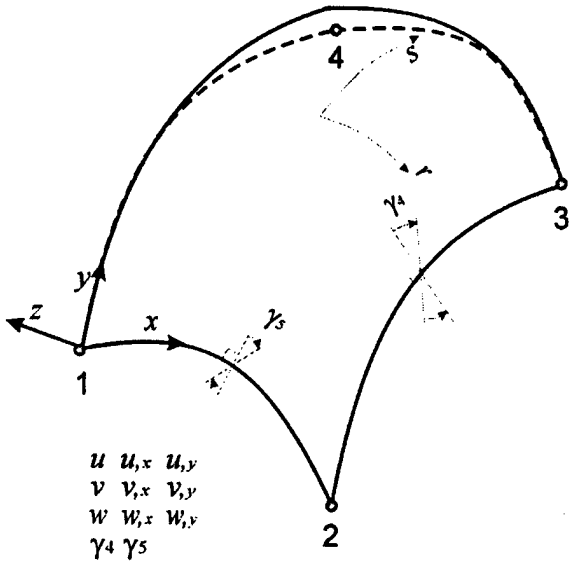

Figure 3: 44 DOF Shell Element

expressed using direction cosines. In Figure (4), the vector $\overline{A}$ is drawn from an arbitrary point P in space and will be referred to a set of unprimed Cartesian coordinate axes with the origin at O, and to a set of primed coordinated axes with the origin at O'. Both sets of axes may be translated without rotation to the common origin at P. It is more convenient to summarize these sets of direction cosines in tabular form as shown in Table 1.

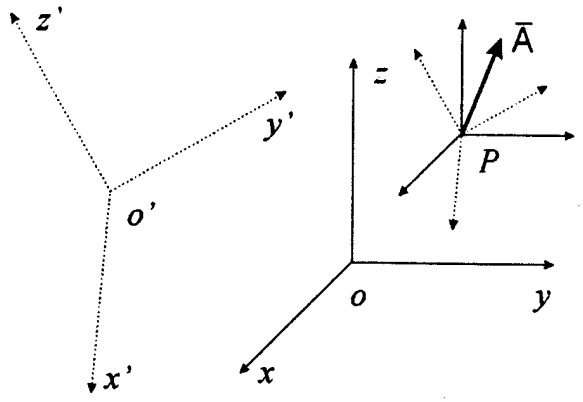

Figure 4: Representation of a vector in two sets of coordinate axes with a different orientation

	x	y	z
x'	l_1	m_1	n_1
y'	l_2	m_2	n_2
z'	l_3	m_3	n_3

Table 1: Direction Cosines between two coordinate axes.

Then, the transformation matrix

$$[\Lambda] = \begin{bmatrix} l_1 & m_1 & n_1 \\ l_2 & m_2 & n_2 \\ l_3 & m_3 & n_3 \end{bmatrix} \tag{22}$$

yielding

$$\begin{Bmatrix} u' \\ v' \\ w' \end{Bmatrix} = [\Lambda] \begin{Bmatrix} u \\ v \\ w \end{Bmatrix} \tag{23}$$

Now, the nodal degree of freedoms of one of the four noded element is

$$\begin{Bmatrix} u' \\ u',_1 \\ u',_2 \\ v' \\ v',_1 \\ v',_2 \\ w' \\ w',_1 \\ w',_2 \\ \gamma'_4 \\ \gamma'_5 \end{Bmatrix} = \underbrace{\begin{bmatrix} l_1 & 0 & 0 & m_1 & 0 & 0 & n_1 & 0 & 0 & 0 & 0 \\ 0 & l_1l_1 & l_1m_1 & 0 & m_1l_1 & m_1m_1 & 0 & n_1l_1 & n_1m_1 & 0 & 0 \\ 0 & l_1l_2 & l_1m_2 & 0 & m_1l_2 & m_1m_2 & 0 & n_1l_2 & n_1m_2 & 0 & 0 \\ l_2 & 0 & 0 & m_2 & 0 & 0 & n_2 & 0 & 0 & 0 & 0 \\ 0 & l_2l_1 & l_2m_1 & 0 & m_2l_1 & m_2m_1 & 0 & n_2l_1 & n_2m_1 & 0 & 0 \\ 0 & l_2l_2 & l_2m_2 & 0 & m_2l_2 & m_2m_2 & 0 & n_2l_2 & n_2m_2 & 0 & 0 \\ l_3 & 0 & 0 & m_3 & 0 & 0 & n_3 & 0 & 0 & 0 & 0 \\ 0 & l_3l_1 & l_3m_1 & 0 & m_3l_1 & m_3m_1 & 0 & n_3l_1 & n_3m_1 & 0 & 0 \\ 0 & l_3l_2 & l_3m_2 & 0 & m_3l_2 & m_3m_2 & 0 & n_3l_2 & n_3m_2 & 0 & 0 \\ 0 & 0 & 0 & 0 & 0 & 0 & 0 & 0 & 0 & 1 & 0 \\ 0 & 0 & 0 & 0 & 0 & 0 & 0 & 0 & 0 & 0 & 1 \end{bmatrix}}_{\Xi'} \begin{Bmatrix} u \\ u,_1 \\ u,_2 \\ v \\ v,_1 \\ v,_2 \\ w \\ w,_1 \\ w,_2 \\ \gamma \\ \gamma \end{Bmatrix} \tag{24}$$

Because of the fact;

$$\frac{\partial u}{\partial x'} = \frac{\partial u}{\partial x}\frac{\partial x}{\partial x'} + \frac{\partial u}{\partial y}\frac{\partial y}{\partial x'} + \frac{\partial u}{\partial z}\frac{\partial z}{\partial x'} = l_1\, u_{,x} + m_1\, u_{,y} + n_1 u_{,z} \tag{25}$$

$$\frac{\partial u'}{\partial x'} = \frac{\partial u'}{\partial x}\overbrace{\frac{\partial x}{\partial x'}}^{l_1} + \frac{\partial u'}{\partial y}\overbrace{\frac{\partial y}{\partial x'}}^{m_1} + \overbrace{\frac{\partial u'}{\partial z}\frac{\partial z}{\partial x'}}^{0} \tag{26}$$

$$= l_1(l_1 u + m_1 v + n_1 w)_{,x} + m_1(l_1 u + m_1 v + n_1 w)_{,y}$$

$$= l_1 l_1 u_{,x} + m_1 l_1 u_{,y} + m_1 l_1 v_{,x} + m_1 m_1 v_{,y} + n_1 l_1 w_{,x} + n_1 m_1 w_{,y}$$

$$\frac{\partial v}{\partial x'} = \frac{\partial v}{\partial x}\frac{\partial x}{\partial x'} + \frac{\partial v}{\partial y}\frac{\partial y}{\partial x'} + \frac{\partial v}{\partial z}\frac{\partial z}{\partial x'} = l_1\, v_{,x} + m_1\, v_{,y} + n_1 v_{,z} \tag{27}$$

etc.

The transformation matrix can be expressed for the 44 DOF element as follows

$$\underset{44\times 44}{[T]} = \begin{bmatrix} \Xi' & [0] & [0] & [0] \\ [0] & \Xi' & [0] & [0] \\ [0] & [0] & \Xi' & [0] \\ [0] & [0] & [0] & \Xi' \end{bmatrix} \tag{28}$$

where [0] is 11 × 11 null matrix in which all the component of matrix are zero. Equation (19) can now be expressed as

$$[K_\alpha]\,[T]\,\{u_x\} = \{R_\alpha\}\,. \tag{29}$$

Multiply both sides of the equation (29) by $[T]^{-1} = [T]^T$ yields

$$\underbrace{[T]^T [K_\alpha] [T]}_{K_x} \{u_x\} = \underbrace{[T]^T \{R_\alpha\}}_{R_x} . \tag{30}$$

where

$$K_x = [T]^T [K_\alpha] [T] \text{ and } R_x = [T]^T \{R_\alpha\} .$$

The Jaumann strain $\{B\}$ is a function of u_α which is $\{B\} = \{B(u_\alpha)\}$. It can be expressed in global Cartesian coordinate system using relationships

$$B'_{ij} = l_{ik} l_{jl} B_{kl}$$

(l_{ij} = direction cosines between the local and global coordinate systems).

And Jaumann stress J' ,which is function of Jaumann strain B' can also be expressed as

$$J'_{ij} = l_{ik} l_{jl} J_{kl}.$$

2.3 Nonconservative Loading Case in JAGS

It is required that the loading system considered in an antenna analysis be directed normal to the deformed surface. Thus, for this to occur one must consider nonconservative loading equations for evaluation. The loading must be applied in increments normal to the surface.

First express the stiffness matrix for the ith load increment as;

$$[K_n] = [K_i] + [\triangle K]_n \tag{31}$$

note $[K_i]$ can be a nonlinear stiffness matrix. and $[\triangle K]_n = dK_n = \left[\frac{\partial K_n}{\partial u_i} du_i\right]$. (For example $K_{11} = 3\left(u_1^2 + u_2^2\right)$ then $dK_{11} = 3\left(2u_1 du_1 + 2u_2 du_2\right)$. The equilibrium equation

$$[K]\{u\} = \{R\} \tag{32}$$

can be replaced by

$$\left([K] + [\triangle K]_n\right)\left(\{u\} + \{\triangle u_n\}\right) = \{R\} + \{\triangle R_n.\} \tag{33}$$

resulting in

$$[K]\{u\} + [K]\{\triangle u_n\} + [\triangle K_n]\{u\} + [\triangle K_n]\{\triangle u_n\} = \{R\} + \{\triangle R_n\} \tag{34}$$

The term $[\triangle K_n]\ \{\triangle u_n\}$is H.O.T., so we can ignore it. Equation (34) reduces to

$$[K]\{u\} + [K]\{\triangle u_n\} + [\triangle K_n]\{u\} = \{\triangle R_n\} + \{R\}. \tag{35}$$

Since $[K]\{u\} = \{R\}$, one can subtract these terms out of the solution in order to find a resulting new incremental equation of state. The Newton-Ralphson

Technique can be used to solve this nonlinear set of equations giving

$$[K_T]\,\delta\{\Delta u\} = \{\Delta R_n\} - [K]\{\Delta u_n\} + [\Delta K_n]\{u\} \tag{36}$$

where $K_T = \frac{\partial}{\partial \Delta u_n}\left([\Delta K_n]\{u\} + [K]\{\Delta u_n\}\right)\delta\{\Delta u_n\}$ (referred to as the tangent stiffness matrix). The terms $\left(\frac{\partial}{\partial\{\Delta u_n\}}[\Delta K_n]\{u\}\right)$ are evaluated by considering

$$\psi = [\Delta K]\{u\} + [K]\{\Delta u_n\} - \{\Delta R_n\} = 0, \tag{37}$$

which is the incremental equilibrium relation.

There are i-equations with i-DOF, then the expression using the index notation is

$$\psi_i = \Delta K_{ij}\, u_j \quad \text{and } d\psi_i = \widetilde{K_{ij}}\, u_j \tag{38}$$

where

$$\widetilde{K_{ij}} = (\Delta K_{in}\, u_n)_{,j}\,. \tag{39}$$

Therefore

$$K_T = [(\Delta K_{in}\, u_n)_{,j} + K]\ \delta\{\Delta u_n\} \tag{40}$$

For example, let's consider the simple two dimensional case,

$$K_{11}\,u_1 + K_{12}\,u_2 = R_1; \text{thus } \psi_1 = K_{11}\,u_1 + K_{12}\,u_2 - R_1 = 0 \tag{41}$$

$$K_{21}\,u_1 + K_{22}\,u_2 = R_2; \text{thus } \psi_2 = K_{21}\,u_1 + K_{22}\,u_2 - R_2 = 0 \tag{42}$$

Then,

$$\frac{\partial \psi_1}{\partial u_1} = \frac{\partial (K_{11}\, u_1)}{\partial u_1} + \frac{\partial (K_{12}\, u_2)}{\partial u_1} = \frac{\partial (K_{1n}\, u_n)}{\partial u_1}; \frac{\partial \psi_1}{\partial u_2} = \frac{\partial (K_{1n}\, u_n)}{\partial u_2} \tag{43}$$

$$\frac{\partial \psi_2}{\partial u_1} = \frac{\partial (K_{21}\, u_1)}{\partial u_1} + \frac{\partial (K_{22}\, u_2)}{\partial u_1} = \frac{\partial (K_{2n}\, u_n)}{\partial u_1}; \frac{\partial \psi_2}{\partial u_2} = \frac{\partial (K_{2n}\, u_n)}{\partial u_2} \tag{44}$$

If we use the modified Newton-Raphson technique, then $K\ \delta\triangle u_{n_{i+1}} = \triangle R_n - K\triangle u_{n_i} + \triangle K_{n_i}\, u_i$ can be used to evaluate $\delta\triangle u_{n_{i+1}}$. The value of $\triangle u_{n_{i+1}}$ (normal increment of displacement for the $i+1$ increment) $= \triangle u_{n_i} + \delta\triangle u_{n_{i+1}}$. The satisfaction of the incremental state of equilibrium is carried out within an established tolerance.

3 Application

Several attempts have been made to compare the method of the analysis of the total Lagrangian theory based on JAGS, and the Eulerian based theory defined by ABAQUS. Three cases have been performed. The first case was cylindrical shell acting under a concentrated transverse load as in Figure 5. This case depicts a shell panel undergoing movement which includes an instability or collapse point. Thus, geometric nonlinear displacement and rotation can occur. This usually is displayed in a problem of this form by showing a load vs. displacement curve for the degree of freedom at the applied force.

There are two regions for this type of curve. The rising or stable region and the descending or unstable region. Each point in the plot represents an equilibrium state.

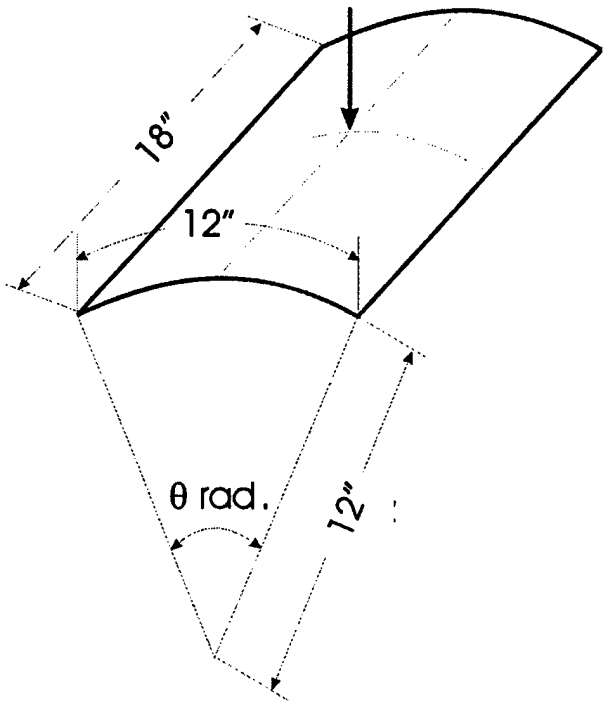

Figure 5: Simply supported point loaded cylinderical shell

The material properties are described as in Table 2. The shell properties were modeled using a Hercules AS4-3501-6 graphite epoxy composite with

E_1	E_2	E_{12}	G_{13}	G_{23}	ν_{12}
18.844 (10^6)	1.468 (10^6)	0.91 (10^6)	0.91 (10^6)	0.45 (10^6)	0.26

Table 2: Material Properties of a Hercules AS4-3501-6 graphite epoxy composite(unit psi)

the following conditions; condition1: dimensions of θ =1 radian, 24 plies $[0_6/90_6]_s$ and 0.12 in. thickness; condition2: θ =1 radian, 12 plies $[0_3/90_3]_s$ and 0.6 in. thickness; ; condition 3: θ =0.5 radian 48 plies $[0_6/90_6]_{2s}$ and 0.24 in. thickness. A (176 nodes, 7x7 Elements) quarter symmetry model was used. Results are shown in Figure 6, 7 and 8.

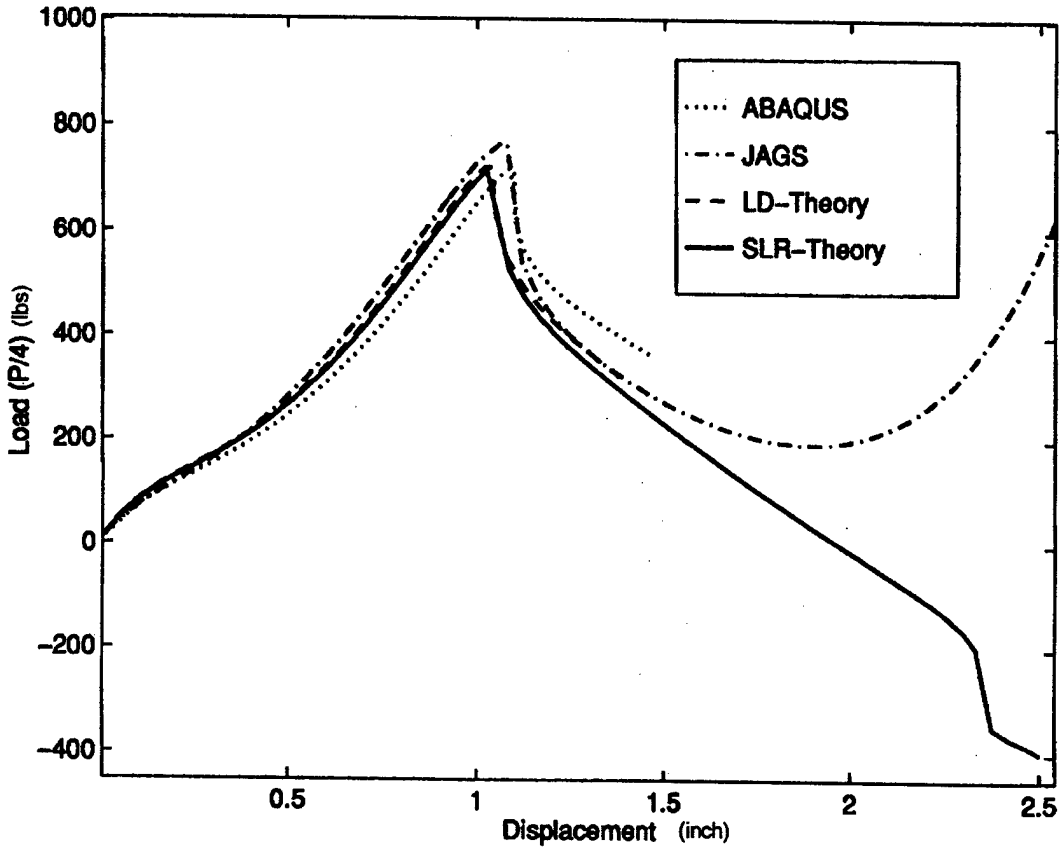

Figure 6: Cylindrical Shell (R=12 in. $\theta = 1$ Radian, 24 Plies)

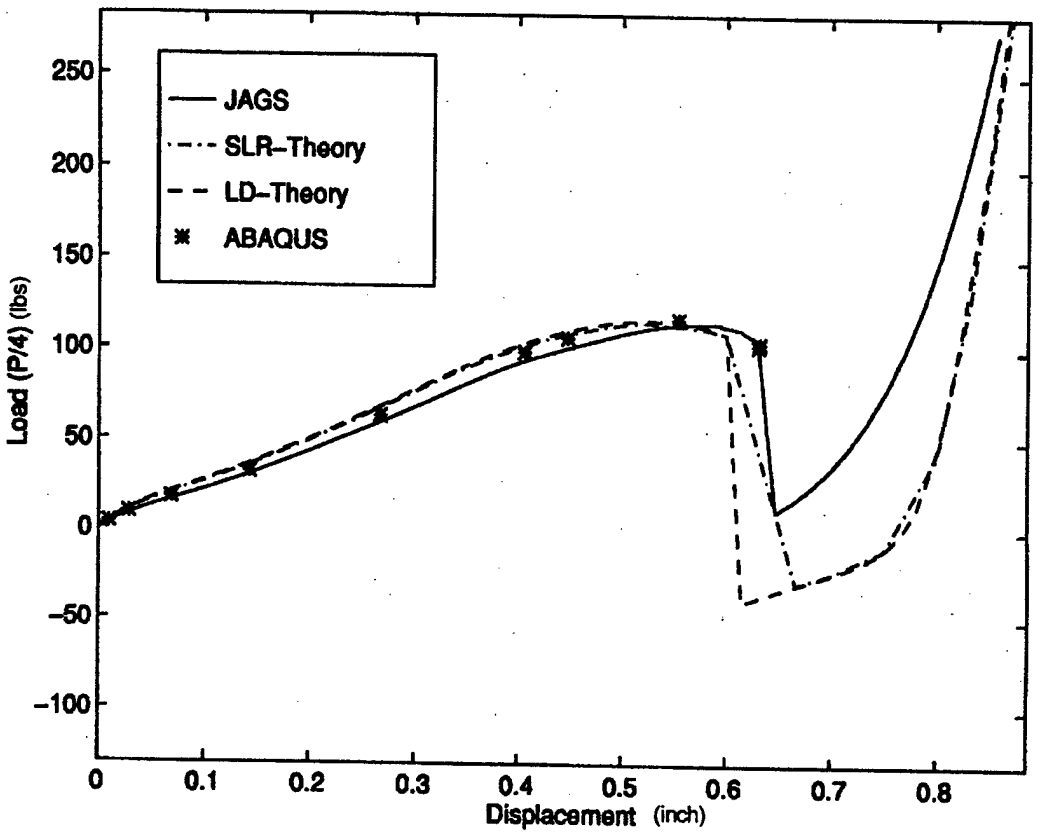

Figure 7: Cylindrical Shell (R=12 in. $\theta = 0.5$ Radian, 12 Plies)

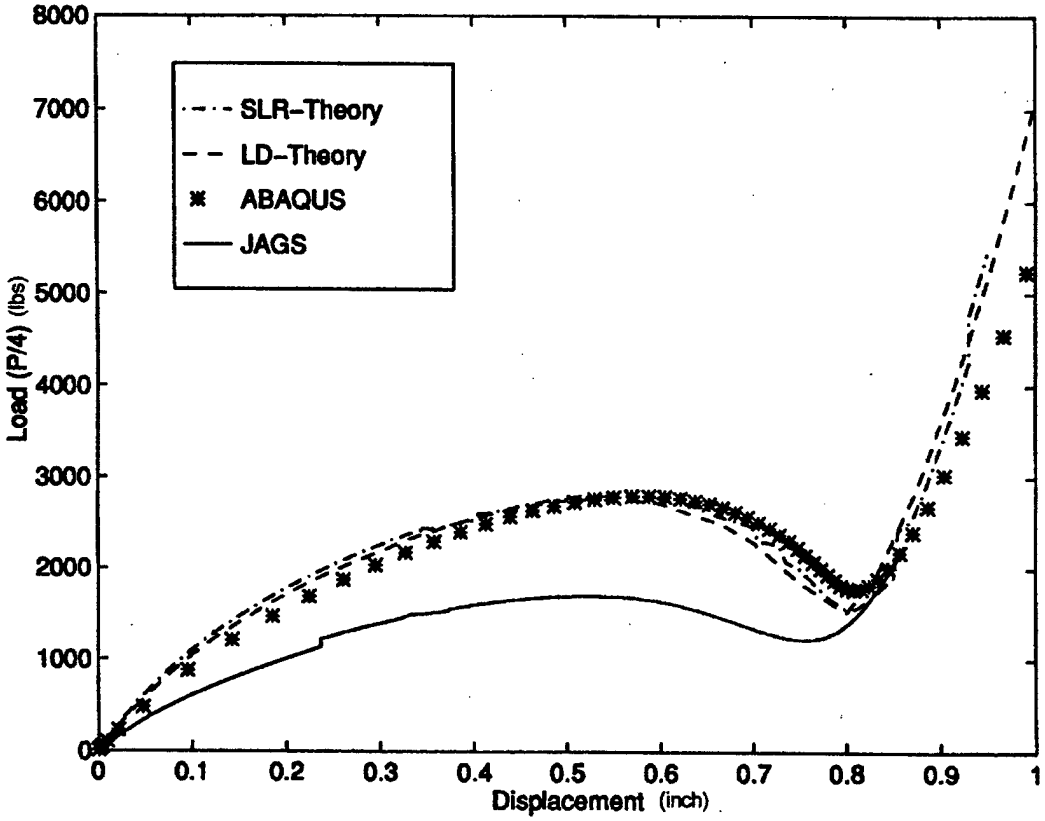

Figure 8: Cylindrical Shell (R=12 in. $\theta = 0.5$ Radian, 48 Plies)

From Figure 6, in the case of a moderate thickness shell, JAGS, ABAQUS. and LDLR give similar results up to and beyond collapse. The SLR theory starts to depict a more flexible structure in the unstable region. As we described in theory part both LDLR and SLR are Lagrangian based and employing 2nd Piola-Kirchhoff stresses and Green strain. The difference in SLR theory assumes small angle approximations. Because the thickness isn't large enough to create through the thickness shear effects, the resulting value of JAGS, ABAQUS, SLR and LDLR are quite close. From Figure 7, in case of the very thin shallow shell, all of the results are reasonably close. Finally, from Figure 8, for the shallow and thick shell case, one can recognize a significant difference between JAGS and the other programs and their theories. This difference is one of the major characteristics of the JAGS program. It can represent through the thickness shear stresses with the approximate continuities better than any of the other theories. SLR doesn't include a through the thickness shear stress compatibility. It assumes parabolic shear strain (it assumes third order shear deformation). LDLR and ABAQUS assumes 1st order shear deformation and neither of these theories consider direct through the thickness shear except the JAGS theories (based on corotational theories, assumes higher order shear deformation).

thickness	E	ν	radius
0.0127 mm	5.516 Gpa	0.3	1.5 m

Table 3: Geometrical Properties of the Shell Structure (Unit psi)

A second model studied was a circular disk (shown in Figure 9) with simply supported boundaries conditions under transverse pressure. This problem has been solved using ABAQUS and compared to the results of Greschik et al.[4] [5]. It still has to be run using the JAGS program. The material properties are listed in Table 3.

Finally, the third model considered is a parabolic shell shown as a dotted line in Figure 9. (This problem still has to be run using JAGS and was only runs using ABAQUS. The results were compared with Greschik et al. [4] [5]). Figure 10 shows 930 S8R type elements for the shell model. The same material properties have been used as in the membrane disk except it follows parabolic curves (it depends on f/D; where f represents the parabolic focal length and D is diameter of parabolic disk). The magnitude of z_{ctr} characterize the shell's center vertical distance. The vertical distance z_{ctr} is 0 for flat disk and 7.376 inches for parabolic membrane shell when f/D ratio is

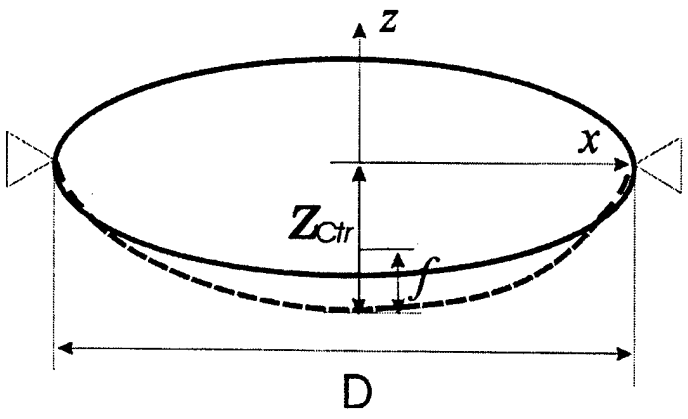

Figure 9: Simply supported Disk and Parabolic shell under transverse pressure

1. The equation of parabolic disk can expressed as $z = \frac{x^2 z_{ctr}}{\left(\frac{D}{2}\right)^2} - z_{ctr}$. The radial and circumferential stress components for node 93 (at the boundary near edge) under an increasing internal pressure is shown in Figure 11 for the circular membrane, and the displacement at the center according to the increasing pressure is showing in Figure12. One should note the nonlinear characteristics. ABAQUS does have the capability of incrementally increasing the pressure and maintaining its direction normal to the deforming surface. Thus the nonconservative capability was implemented in running the problems. The parabolic shell is a good initial depiction of the antenna surface, and thus it becomes important to characterize the observed results for

low loading pressures. Figures 13, 14 depict the stress components at node 93 for the parabolic shell geometry and the center displacement in which the supports were assumed to be pinned (radial, tangential and z direction is constrained as fixed). These two figures show that the support condition creates the type of stress field recognized for its linear membrane character. The tangential stress is linearly increasing and is continuously showing a tension. The center deflection is also purely linear relative to the load as shown in Figure 14. In the next condition considered, the radial constraint is removed. The deep shell with a $f/D = 1$ indicates that a compressive stress component occurs in the tangential or hoop direction and Figures 15 - 18 are verification of this stress. At node 185 negative hoop stresses increase when the loading increases. The location of nodes 93 and 185 are described in the Figure 10. Figures 19 - 22 represent the fact that radial and hoop stresses change according to coordinate angle, (where the coordinate angle is measured counter clockwise with respect to the x-axis; x-axis is 0 and y-axis is 90 degree). Negative hoop stresses exist. It can also be noticed that close to the supports the compressive hoop stress region decreases with respect to a load increase as shown in Figures 21 and 22. In fact, at a load of 5.9531×10^{-4} psi, the shell shows a very small value of compressive hoop

stress. Figure 23 and 24 represent the hoop stress value along a coordinate angle of close to zero degrees. One can observe the region of negative values of this stress component and their magnitude at load 1.2711×10^{-4} and 3.1777×10^{-4} *psi*. It becomes apparent that the boundary restraint is very important in relationship to the membrane stress component.

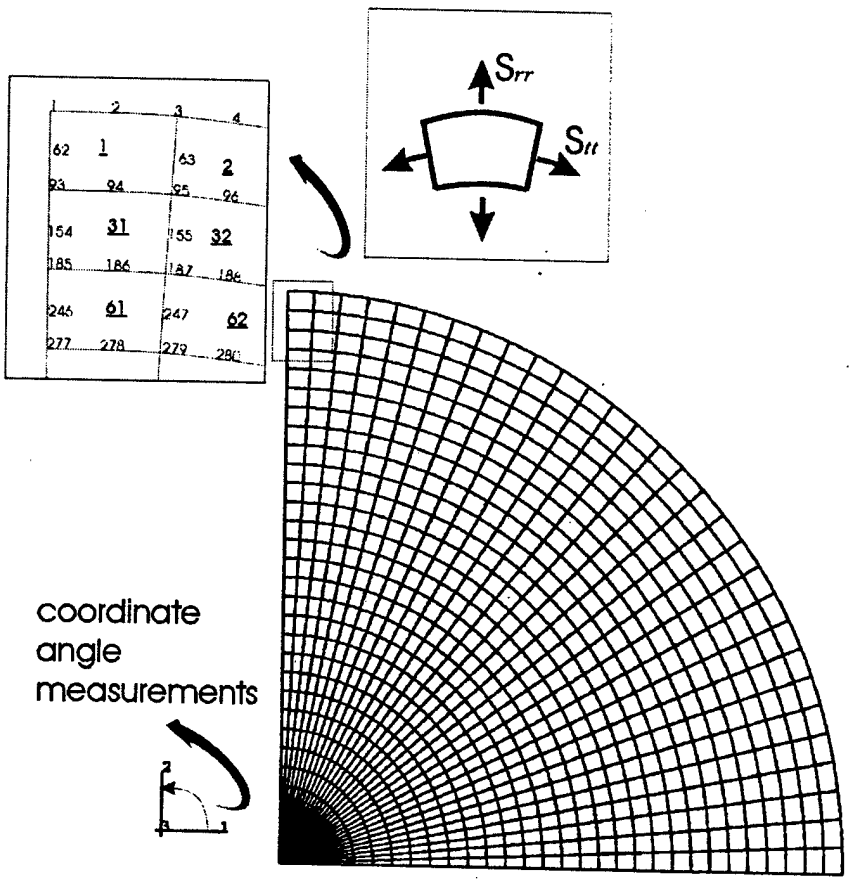

Figure 10: Node numbers and Element numbers of Flat disk and Parabolic membrane shell geometry. (regular numbers represent node numbers and underlined numbers represent element numbers) Representation of Radial stress Srr and Tangential stress Stt.

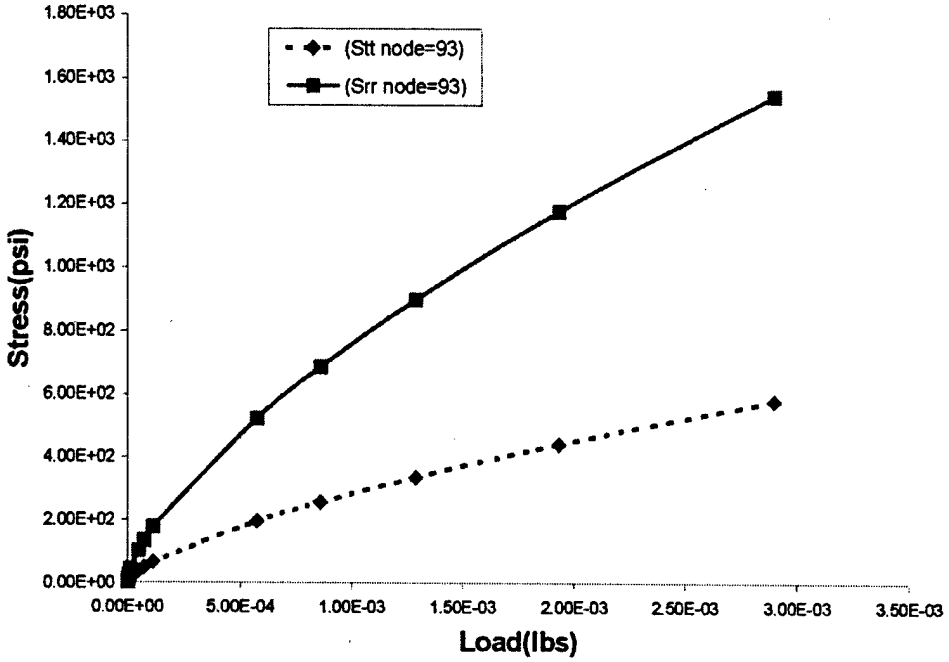

Figure 11: Radial Stress(Srr) and Tangential Stress(Stt) vs. Load Curve (Initially flat disk with pinned support case).

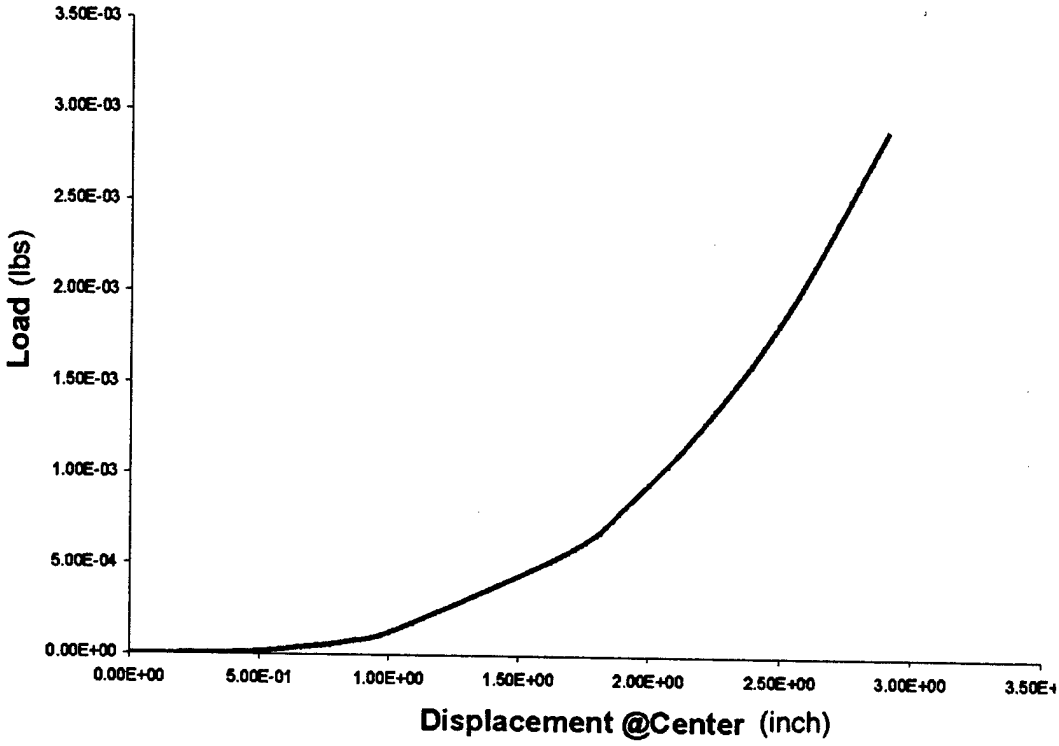

Figure 12: Load-Displacement Curve @Center (Initially flat disk with pinned support case).

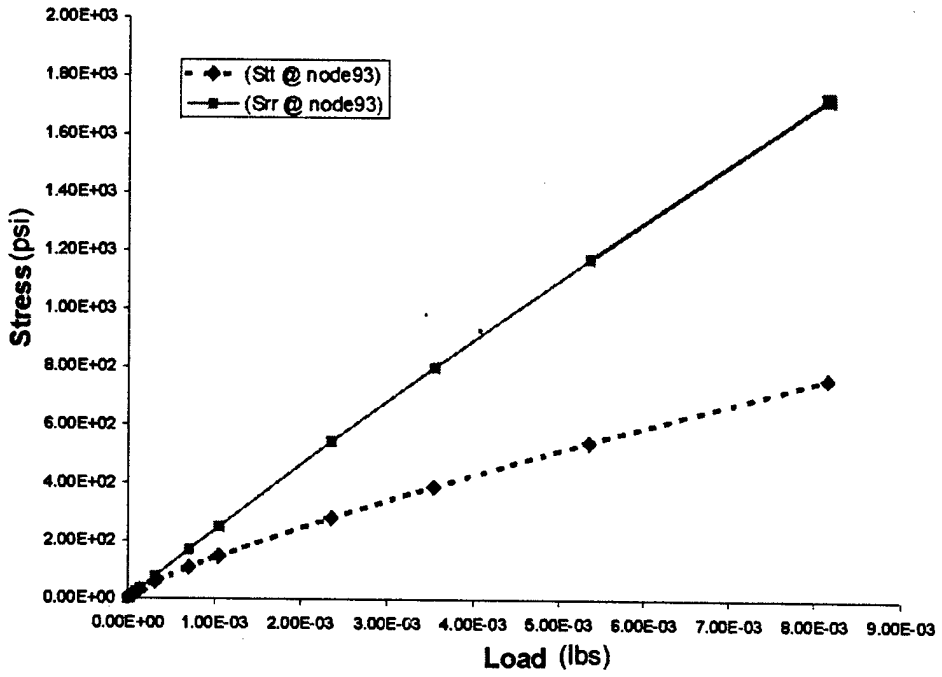

Figure 13: Radial Stress(Srr) and Tangential Stress(Stt) vs. Load Curve (Initially Parabolic membrane shell geometry ($f/D = 1$) with pinned support case)

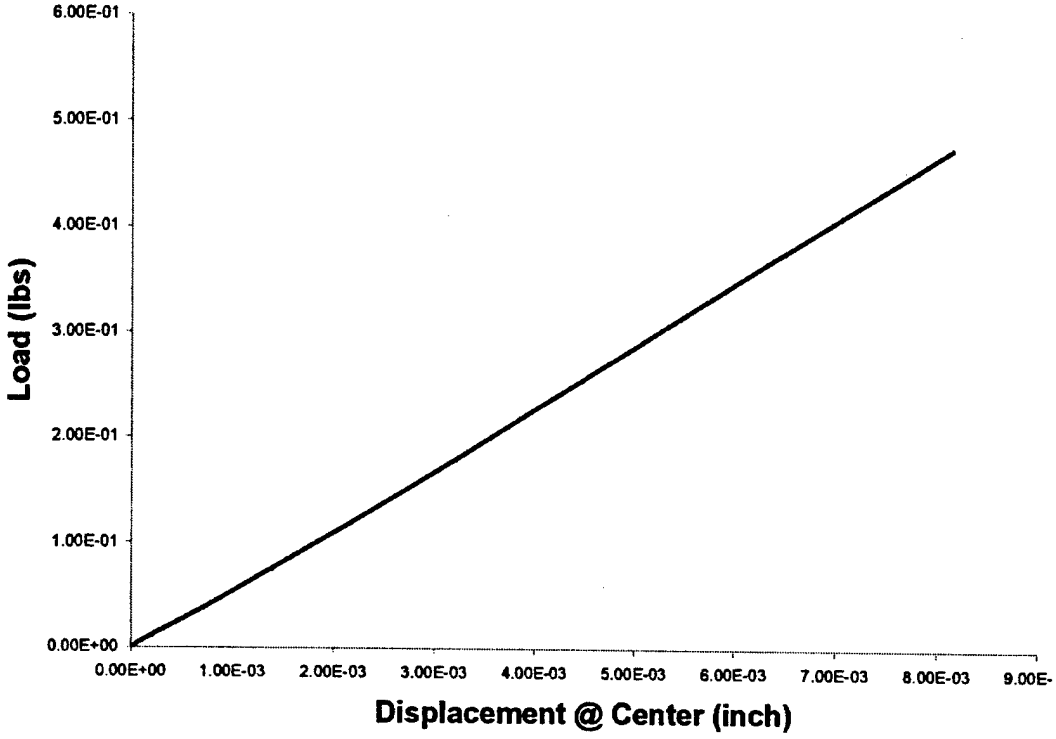

Figure 14: Load-Displacement Curve @Center (Initially Parabolic membrane shell geometry ($f/D = 1$) with pinned support case).

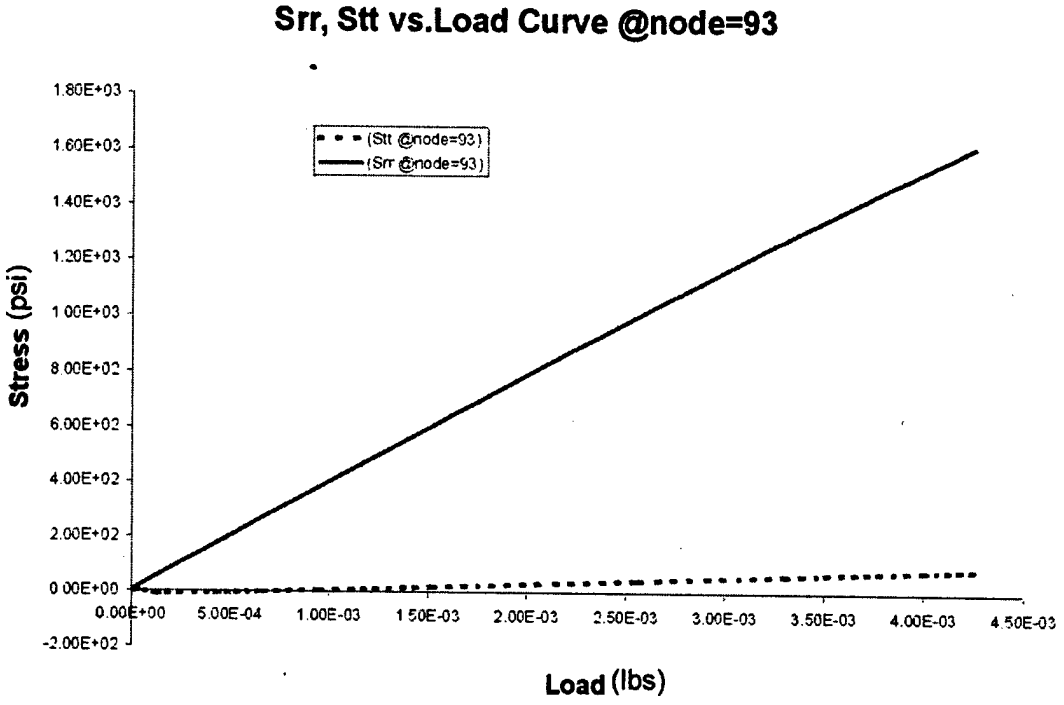

Figure 15: Radial Stress(Srr) and Tangential Stress(Stt) vs. Load Curve @ node 93 (Initially Parabolic membrane shell geometry ($f/D = 1$) with no radial constraint-pinned support case).

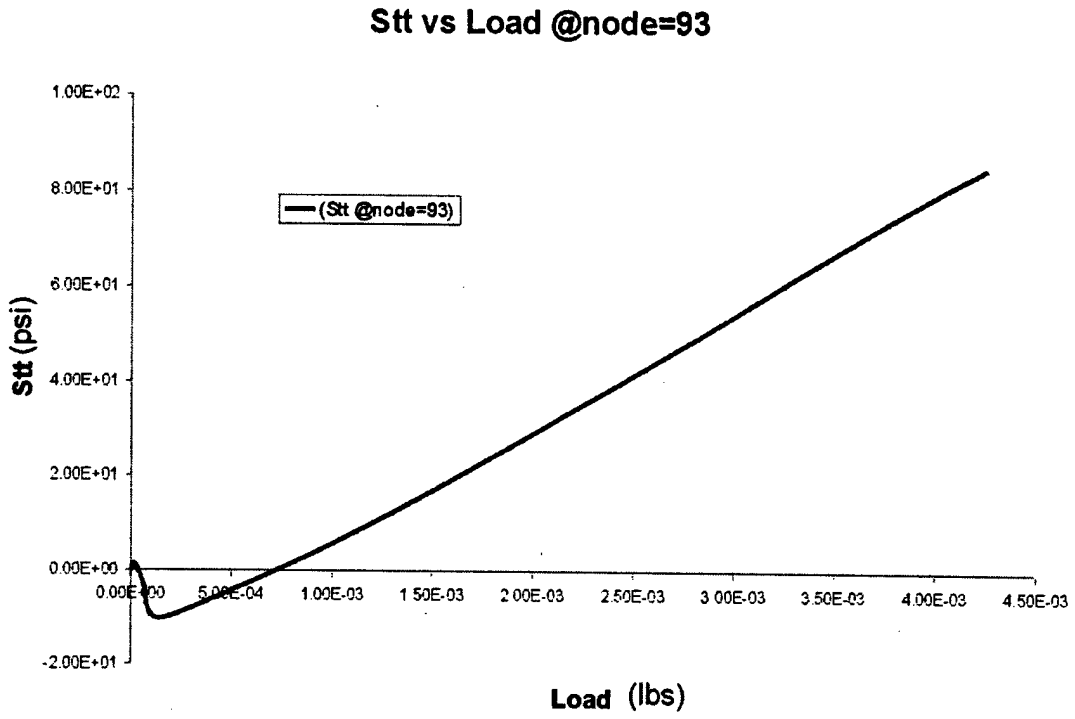

Figure 16: Detailed figure of Tangential Stress(Stt) vs. Load Curve @ node 93

(Initially Parabolic membrane shell geometry ($f/D = 1$) with no radial constraint-pinned support case).

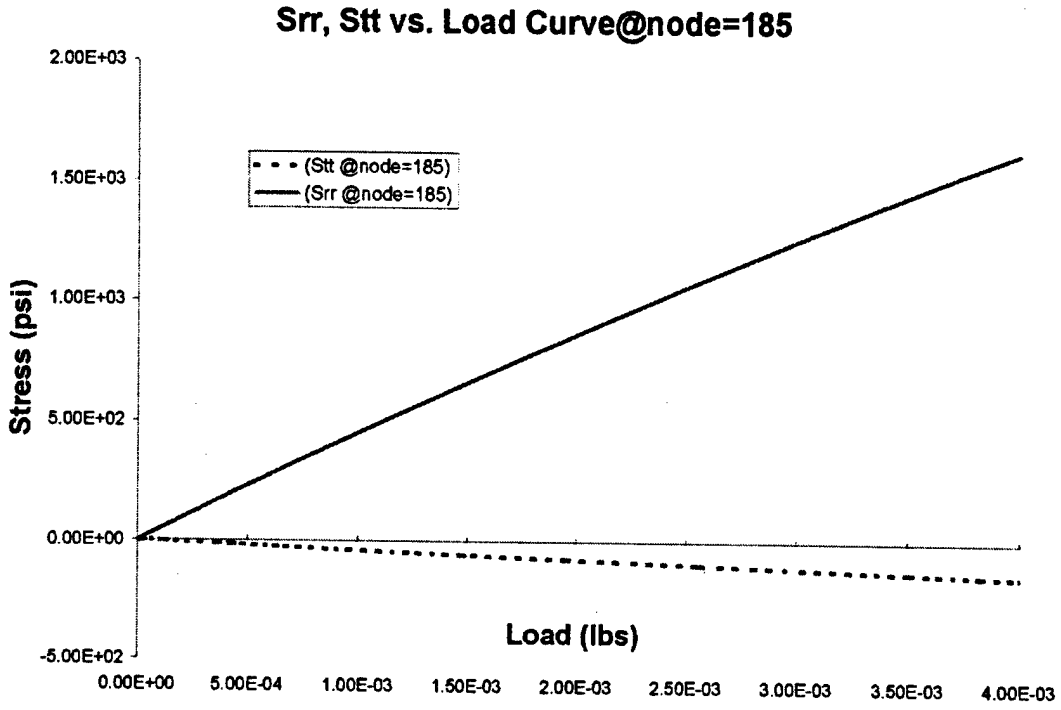

Figure 17: Radial Stress(Srr) and Tangential Stress(Stt) vs. Load Curve @ node185

(Initially Parabolic membrane shell geometry ($f/D = 1$) with no radial constraint-pinned support case).

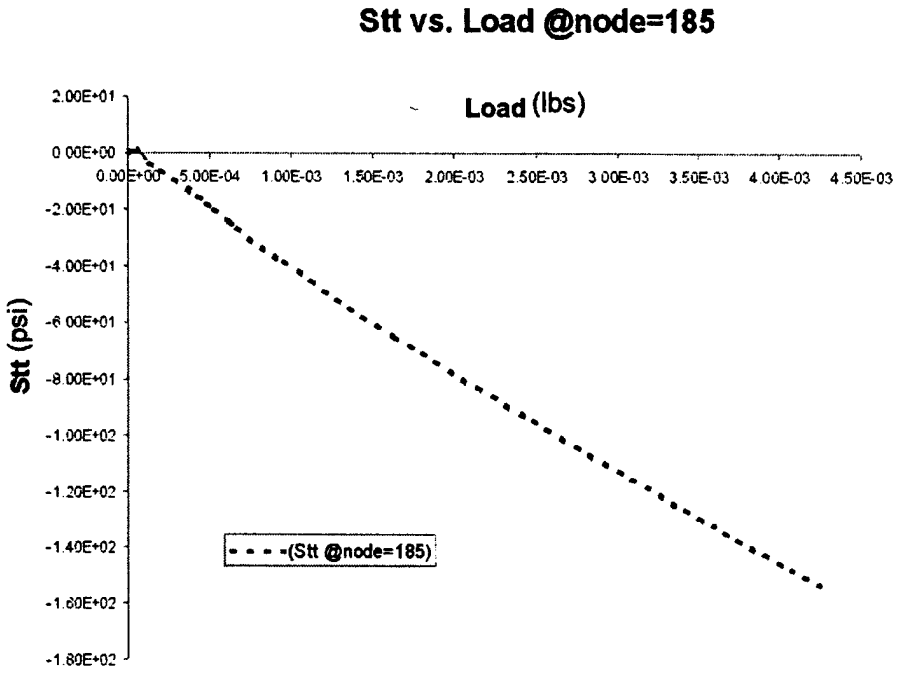

Figure 18: Detailed figure of Tangential Stress(Stt) vs. Load Curve

(Initially Parabolic membrane shell geometry ($f/D = 1$) with no radial constraint-pinned support case)

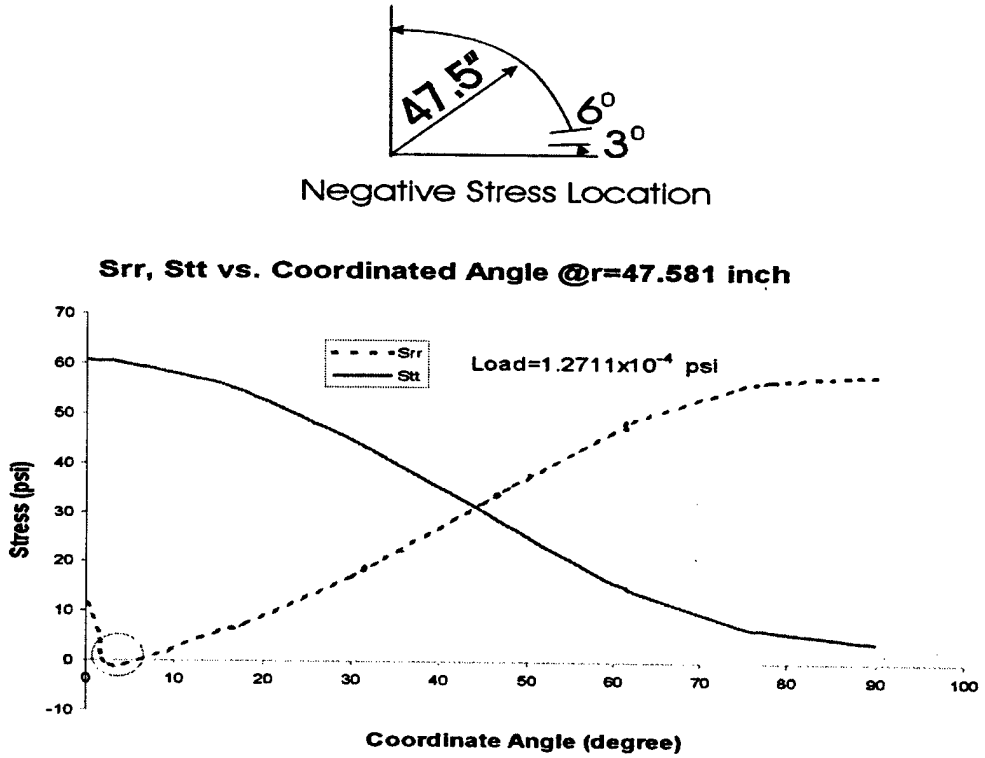

Figure 19: Radial Stress(Srr) and Tangential Stress(Stt) @ radial distance=47.581 inch and load= 1.2711×10^{-4} psi

(Initially Parabolic membrane shell geometry ($f/D = 1$) with no radial constraint-pinned support case).

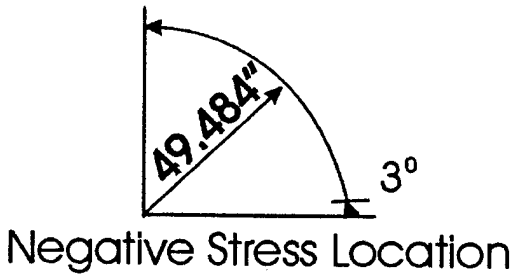

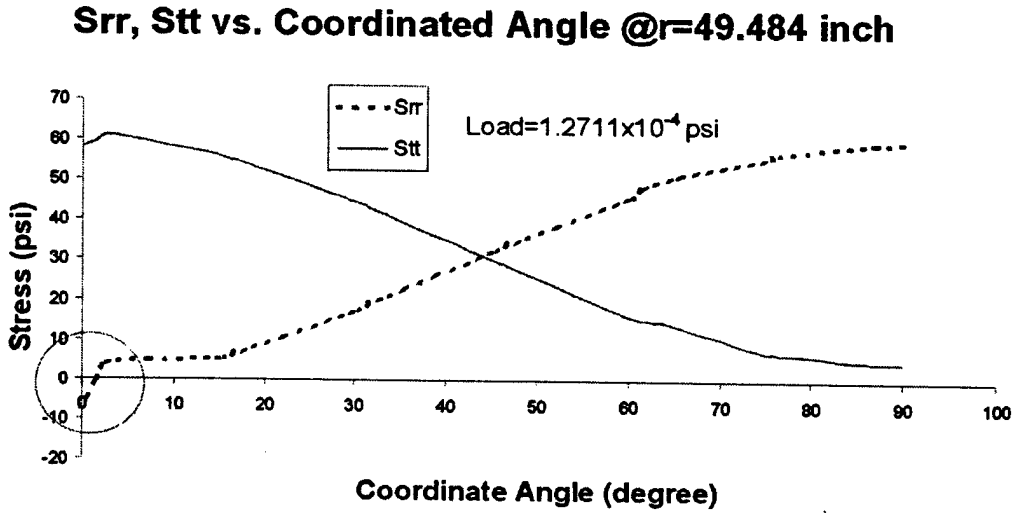

Figure 20: Radial Stress(Srr) and Tangential Stress(Stt) @ radial distance=49.484 inch and load= 1.2711×10^{-4} psi

(Initially Parabolic membrane shell geometry ($f/D = 1$) with no radial constraint-pinned support case).

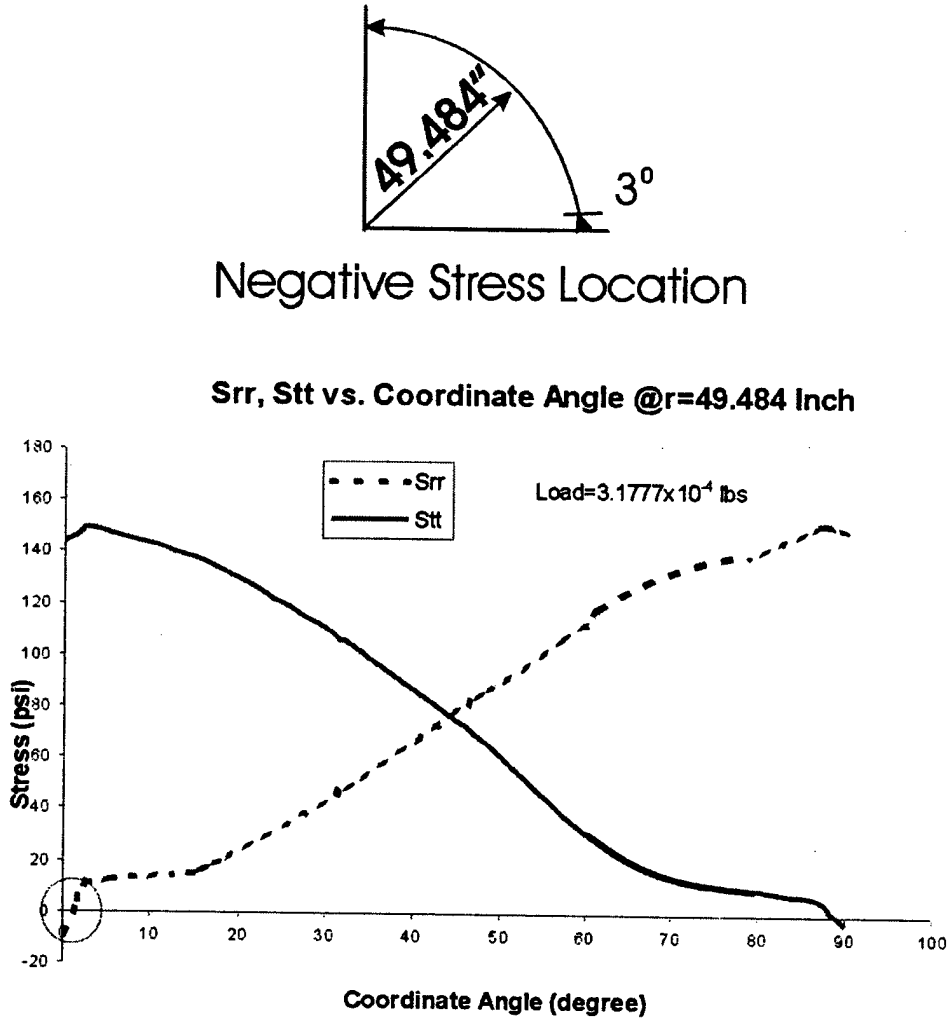

Figure 21: Radial Stress(Srr) and Tangential Stress(Stt) @ radial distance=49.484 inch and load= 3.1777×10^{-4} psi

(Initially Parabolic membrane shell geometry ($f/D = 1$) with no radial constraint-pinned support case).

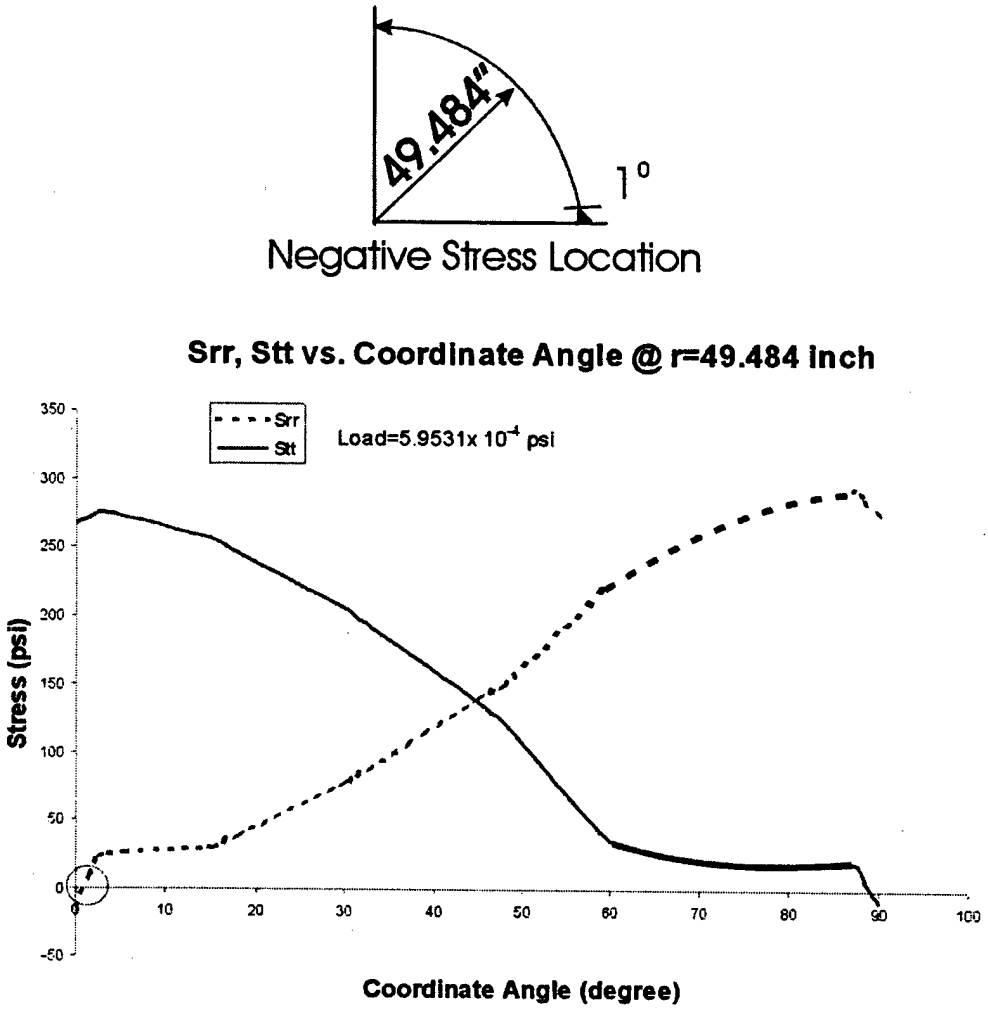

Figure 22: Radial Stress(Srr) and Tangential Stress(Stt) vs. Loads Curve @ radial distance=49.484 inch and load= 5.9531×10^{-4} psi

(Initially Parabolic membrane shell geometry ($f/D = 1$) with no radial constraint-pinned support case).

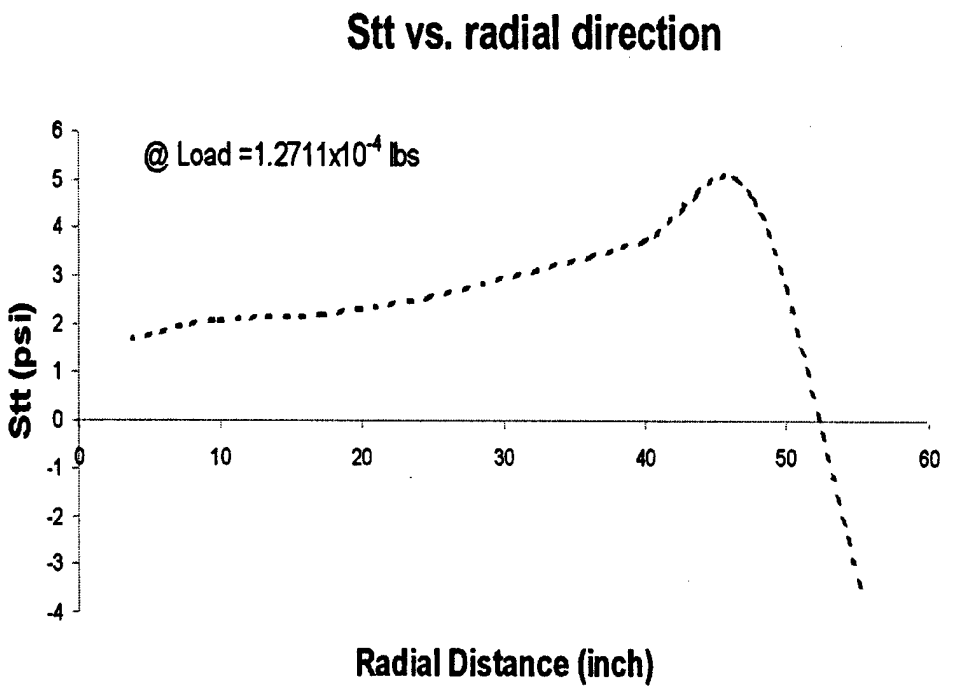

Figure 23: Tangential Stress vs. Radial Distance @ load $= 1.2711 \times 10^{-4} psi$.

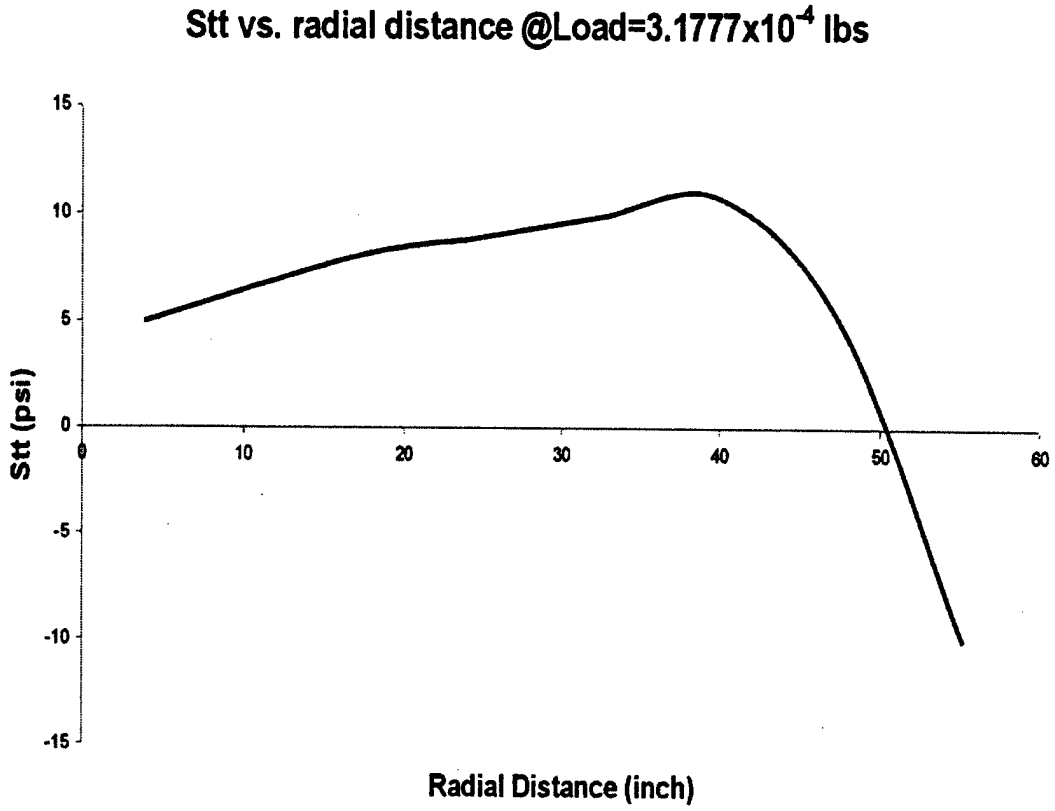

Figure 24: Tangential Stress vs. Radial Distance @ load = 3.1777 $10^{-4} psi$.

4 Further Research

This effort is directed toward the development of a program that is specifically designed to carry out the nonlinear analysis of antenna structures. JAGS is the in-house program worked upon for this purpose. So far we have characterized an individual panel, a disk and a parabolic shell structure under various loadings using ABAQUS. The JAGS program has been compared to ABAQUS for the panel. The equations have been developed for nonconservative loading to be implemented in JAGS. Also, the transformation relations needed for a generalized global set of elements was developed and needs to be implemented in JAGS. Once the new relations for a nonconservative loading and a generalized transformation are implemented in JAGS, the membrane and parabolic shell will be run. The authors will also continue to characterize the antenna structure using ABAQUS. We will next combine two parabolic shells; one concave up and the other concave down joined at their connecting points under internal pressure. This will be followed by including discrete tie rods at specific locations. The final model, that is the global configuration, will be one which includes the parabolic shell configurations joined to a torus through the appropriate tie rod configurations. The torus will be supported a three concentrated points separated by 120 degree. It is apparent that

the most important part of the last scenario is the instability of the torus. The JAGS program results will be compared to ABAQUS throughout the research. As the global model becomes more and more complicated, it has become obvious that the computer intensive feature will be a challenge.

5 Appendix -The Terms in Equation (18)

The shape function matrix in natural coordinates is given by

$$\underset{24\times44}{\mathbf{D}}\ (r,s) = \begin{bmatrix} \underset{6\times3}{\mathbf{H}_1} & \underset{6\times8}{\mathbf{0}} & \underset{6\times3}{\mathbf{H}_2} & \underset{6\times8}{\mathbf{0}} & \underset{6\times3}{\mathbf{H}_3} & \underset{6\times8}{\mathbf{0}} & \underset{6\times3}{\mathbf{H}_4} & \underset{6\times8}{\mathbf{0}} & \\ \underset{6\times3}{\mathbf{0}} & \underset{6\times3}{\mathbf{H}_1} & \underset{6\times8}{\mathbf{0}} & \underset{6\times3}{\mathbf{H}_2} & \underset{6\times8}{\mathbf{0}} & \underset{6\times3}{\mathbf{H}_3} & \underset{6\times8}{\mathbf{0}} & \underset{6\times3}{\mathbf{H}_4} & \underset{6\times5}{\mathbf{0}} \\ \underset{6\times6}{\mathbf{0}} & \underset{6\times3}{\mathbf{H}_1} & \underset{6\times8}{\mathbf{0}} & \underset{6\times3}{\mathbf{H}_2} & \underset{6\times8}{\mathbf{0}} & \underset{6\times3}{\mathbf{H}_3} & \underset{6\times8}{\mathbf{0}} & \underset{6\times3}{\mathbf{H}_4} & \underset{6\times2}{\mathbf{0}} \\ \underset{3\times9}{\mathbf{0}} & \underset{3\times1}{\mathbf{L}_1} & \underset{3\times10}{\mathbf{0}} & \underset{3\times1}{\mathbf{L}_2} & \underset{3\times10}{\mathbf{0}} & \underset{3\times1}{\mathbf{L}_3} & \underset{3\times10}{\mathbf{0}} & \underset{3\times1}{\mathbf{L}_4} & \underset{3\times1}{\mathbf{0}} \\ \underset{3\times10}{\mathbf{0}} & \underset{3\times1}{\mathbf{L}_1} & \underset{3\times10}{\mathbf{0}} & \underset{3\times1}{\mathbf{L}_2} & \underset{3\times10}{\mathbf{0}} & \underset{3\times1}{\mathbf{L}_3} & \underset{3\times1}{\mathbf{L}_0} & \underset{3\times1}{\mathbf{L}_4} & \end{bmatrix} \qquad \text{(A 1)}$$

where

$$\mathbf{H}_k = \begin{bmatrix} \mathcal{H}_1^k & \mathcal{H}_2^k & \mathcal{H}_3^k \\ \mathcal{H}_{1,r}^k & \mathcal{H}_{2,r}^k & \mathcal{H}_{3,r}^k \\ \mathcal{H}_{1,s}^k & \mathcal{H}_{2,s}^k & \mathcal{H}_{3,s}^k \\ \mathcal{H}_{1,rr}^k & \mathcal{H}_{2,rr}^k & 0 \\ \mathcal{H}_{1,rs}^k & \mathcal{H}_{2,rs}^k & \mathcal{H}_{3,rs}^k \\ \mathcal{H}_{1,ss}^k & 0 & \mathcal{H}_{3,ss}^k \end{bmatrix}, \quad \text{and} \quad \mathbf{L}_k = \begin{bmatrix} \mathcal{L}^k \\ \mathcal{L}_{,r}^k \\ \mathcal{L}_{,s}^k \end{bmatrix} \qquad \text{(A2)}$$

The shape functions are given by

$$\mathcal{H}_1^k = (1/8)(1+r_k r)(1+s_k s)\left(2+r_k r+s_k s-r^2-s^2\right) \qquad \text{(A3a)}$$

$$\mathcal{H}_2^k = (a/8)\, r_k (1+r_k r)^2 (r_k r-1)(1+s_k s) \qquad \text{(A3b)}$$

$$\mathcal{H}_3^k = (b/8)\, r_k (1+r_k r)(s_k s-1)(1+s_k s)^2 \qquad \text{(A3c)}$$

$$\mathcal{L}^k = (1/4)(1 + r_k r)(1 + s_k s) \tag{A3d}$$

where 2a and 2b are dimensions along x and y of the rectangular (in curvilinear coordinates) element, and the values of r_k and s_k are determined by the local coordinates(r,s) of the kth node.

A vector$\{\psi\}$ displacement quantities at the reference surface can be expressed as;

$$\{\psi\} = \{(1+e_1)\cos\gamma_{61} - 1,\ (1+e_2)\cos\gamma_{62},\ (1+e_1)\sin\gamma_{61} + (1+e_2)\sin\gamma_{62},$$
$$k_1 - k_1^0,\ k_2 - k_2^0,\ k_6 - k_6^0,\ \gamma_{4,x},\ \gamma_{4,y},\ \gamma_{5,x},\ \gamma_4,\ \gamma_5\}^T \tag{A4}$$

$\{\psi_0\}$ are all known values at q_0 in equation(18).

A expression 12×12 symmetric matrix $[\Phi]$ is

$$[\Phi] = \sum_{i=1}^{N} \int_{z_i}^{z_{i+1}} \left[S^{(i)}\right]^T \left[\overline{Q}^{(i)}\right] \left[S^{(i)}\right] dz \tag{A5}$$

where $\left[\overline{Q}^{(i)}\right]$ is the material transformed stiffness matrix for the ith lamina

from its principal matrix $\left[Q^{(i)}\right]$ and the matrix $\left[S^{(i)}\right]$ is

$$\left[S^{(i)}\right] = \begin{bmatrix} 1 & 0 & 0 & z & 0 & 0 & g_{14}^{(i)} & 0 & g_{15}^{(i)} & 0 & -k_5 g_{24}^{(i)} & -k_5 g_{25}^{(i)} \\ 0 & 1 & 0 & 0 & z & 0 & 0 & g_{24}^{(i)} & 0 & g_{25}^{(i)} & k_4 g_{14}^{(i)} & k_4 g_{15}^{(i)} \\ g_{30}^{(i)} & g_{31}^{(i)} & g_{32}^{(i)} & g_{33}^{(i)} & g_{34}^{(i)} & g_{35}^{(i)} & g_{36}^{(i)} & g_{37}^{(i)} & g_{38}^{(i)} & g_{39}^{(i)} & g_{51}^{(i)} & g_{61}^{(i)} \\ 0 & 0 & 1 & 0 & 0 & z & g_{24}^{(i)} & g_{14}^{(i)} & g_{25}^{(i)} & g_{15}^{(i)} & g_{52}^{(i)} & g_{62}^{(i)} \\ 0 & 0 & 0 & 0 & 0 & 0 & 0 & 0 & 0 & 0 & g_{53}^{(i)} & g_{63}^{(i)} \\ 0 & 0 & 0 & 0 & 0 & 0 & 0 & 0 & 0 & 0 & g_{54}^{(i)} & g_{64}^{(i)} \end{bmatrix} \quad \text{(A6a)}$$

The values of the entries $g_{kl}^{(i)}$ (warping and thickness stretching function) are

$$g_{51}^{(i)} = k_4 g_{41}^{(i)} + k_5 g_{42}^{(i)}, \quad g_{52}^{(i)} = k_5 g_{14}^{(i)} + k_4 g_{24}^{(i)} \quad \text{(A6aa)}$$

$$g_{61}^{(i)} = k_4 g_{43}^{(i)} + k_5 g_{44}^{(i)}, \quad g_{62}^{(i)} = k_5 g_{15}^{(i)} + k_4 g_{25}^{(i)} \quad \text{(A6ab)}$$

$$g_{3j}^{(i)} = a_{3j}^{(i)} + 2b_{3j}^{(i)} z, \; j = 0, .., 9; \; g_{4j}^{(i)} = a_{4j}^{(i)} + 2b_{4j}^{(i)} z, \; j = 1, .., 4 \quad \text{(A6ac)}$$

$$g_{53}^{(i)} = g_{24,z}^{(i)} - (k_2 g_{24} + k_{62} g_{14}), \quad g_{63}^{(i)} = g_{25,z}^{(i)} - (k_2 g_{25} + k_{62} g_{15}) \quad \text{(A6ad)}$$

$$g_{54}^{(i)} = g_{14,z}^{(i)} - (k_{61} g_{24} + k_1 g_{14}), \quad g_{64}^{(i)} = g_{15,z}^{(i)} - (k_{61} g_{25} + k_1 g_{15}) \quad \text{(A6ae)}$$

An element of the $[\Psi]$ *matrix*

To illustrate the content of the $[\Psi]$ matrix, we first consider the displace-

ment gradient vector, $\{U\}$

$$\begin{aligned}\underset{24\times1}{\{U\}} &= \{u; u_{,x}\,; u_{,y}\,; v; v_{,x}\,; v_{,y}\,; v_{,xx}\,; v_{,xy}\,; v_{,yy}\,; \\ &\quad w; w_{,x}\,; w_{,y}\,; w_{,xx}\,; w_{,xy}\,; w_{,yy}\,; \gamma_4; \gamma_{4,x}\,; \gamma_{4,y}\,; \\ &\quad \gamma_5; \gamma_{5,x}\,; \gamma_{5,y}\,\}^T \end{aligned} \tag{A7}$$

and the variation of the vector

$$\delta\{\Psi\} = [\Psi]\,\delta\{U\} \tag{A8}$$

where

$$\Psi_{ij} = [\Psi] = \frac{\partial \Psi_i}{\partial U_j} \tag{A8a}$$

$\boldsymbol{\Psi}(i,j)$ are functions of the global displacements u, v, w and the initial curvature. The terms are generated in mathematica. It can be shown for example that $\boldsymbol{\Psi}(6,4) = \dfrac{\partial \Psi_6}{\partial u_{,xx}}$.

$$\begin{aligned}\boldsymbol{\Psi}(6,4) &= \partial\psi_6/\partial U_4 \\ &= \partial\left(k_6 - k_6^0\right)/\partial u_{,xx} \\ &= \partial\left(k_{61} + k_{62} - k_{61}^0 - k_{62}^0\right)/\partial u_{,xx}\end{aligned} \tag{A9}$$

where $k_{61}$and k_{62} are the scalar quantities representing $-\dfrac{\partial \mathbf{i}_2}{\partial x}\cdot\mathbf{i}_2$ and $-\dfrac{\partial \mathbf{i}_1}{\partial y}\cdot\mathbf{i}_3$ respectively (see Figure 2), and k_{61}^0 for example is the curvature term that yields the $\mathbf{j}_3$ component of the $\dfrac{\partial \mathbf{j}_1}{\partial y_2}$(again see Figure 2).

The results is

$$\Psi(6,4) = \partial\left(-T_{21,x}T_{31} - T_{22,x}T_{32} - T_{23,x}T_{33}\right)/\partial u_{,xx} \qquad \text{(A10)}$$

where the T_{ij} are functions of fiber stretching and the corotational axes at the deformed configuration of a point. This yields the expression for $\Psi(6,4)$ in terms of a numerator and denominator function;

$$\begin{aligned}\Psi(6,4)_N &= c\left(-(ab) + b^2 + d^2\right) \\ &\times\sqrt{a\left(a^5 - 2a^3b + ab^2 + 3a^2d^2 - bd^2 - 2bd^2 - 2\sqrt{a}d^2\sqrt{ab-d^2}\right)} \\ &\times\left(-(c_3c_5) + c_2c_6\right) \qquad \text{(A10a)}\end{aligned}$$

$$\begin{aligned}\Psi(6,4)_D &= \sqrt{a}\sqrt{\left(a^3 - ab + d^2\right)^2}\left(b + \sqrt{ab-d^2}\right) \\ &\times\sqrt{b\left(a^2b - 2ab^2 + b^3 - ad^2 + 3bd^2 - ad^2\sqrt{ab-d^2}\right)} \qquad \text{(A10b)} \\ &\times\sqrt{c_2^2c_4^2 + c_3^2c_4^2 - 2c_1c_2c_4c_5 + c_1^2c_5^2 + c_3^2c_5^2 - 2c_1c_3c_4c_6 + c_1^2c_6^2 + c_2^2c_6^2}\end{aligned}$$

where

$$\begin{aligned}c_1 &= 1 + u_{,x} - vk_5^0 + wk_1^0 \\ c_2 &= v_{,x} - uk_5^0 + wk_{61}^0 \\ c_3 &= w_{,x} - uk_1^0 + vk_{61}^0 \\ c_4 &= u_{,y} - vk_4^0 + wk_{62}^0\end{aligned}$$

$$
\begin{aligned}
c_5 &= 1 + v_{,y} - uk_4^0 + wk_2^0 \qquad \text{(A10c)} \\
c_6 &= w_{,y} - uk_{62}^0 + vk_2^0 \\
a &= \sqrt{c_1^2 + c_2^2 + c_3^2} \\
b &= \sqrt{c_4^2 + c_5^2 + c_6^2} \\
c &= c_1c_4 + c_2c_5 + c_3c_6 \\
d &= 1/\sqrt{ab}
\end{aligned}
$$

All other terms are expressed in detail in Appendix of Greer[14] or refer to Greer and Palazotto[15].

6 References

[1] Stutzman, W. L. and Thiele, G. A., Antenna Theory and Design, John Wiley & Sons, New York, 1981, pp.375-445.

[2] Greer, J. and Palazotto, A. N., Application of A Total Lagrangian Corotational Finite Element Scheme to Inflation of Tire, *International Journal of Solids and Structures,* Vol. 34, NO. 27, 1995a, pp.3547-3573.

[3] Pai, P. F. and Palazotto, A. N., Nonlinear Displacement-Based Finite-Element Analysis of Composite Shells —A New Total Lagrangian For-

mulation. *International Journal of Solids and Structures,* Vol. 32, 1997 pp.3541-3570.

[4] Greschik, G.: Palisoc, A.: Cassapakis, C.: Veal, G. and Mikulas, M. M., Approximating Paraboloids with Axysymmetric Pressurized Membrane, *American Institute of Aeronautics and Astronautics,* Vol.4, pp. 2772-2782.

[5] Greschik, G.: Mikulas, M. M. and Palisoc, A., Approximations and Errors in Pressurized Axisymmetric Membrane Shape Predictions, *American Institute of Aeronautics and Astronautics,* Vol.4, pp. 2761-2771.

[6] Palazotto, A. N. and Dennis,S. T., Nonlinear Analysis of Shell Structures, American Institute of Aeronautics and Astronautics, Inc., Education Series, 1992, pp.21-232.

[7] Gummadi, L. N. B and Palazotto, Nonlinear Large Strain Analysis of Beams and Arches undergoing Large Rotations, *Journal of Engineering Mechanics*, April 1997, pp.394-398.

[8] Gummadi, L. N. B and Palazotto, Finite element analysis of Arches under going large rotations -I: Theoretical comparison, *Finite Elements in Analysis and Design*, 24, 1997, pp.213-235.

[9] Palazotto, A. N., Gummadi, L. N. B and Bailey, J. C., Finite element analysis of Arches under going large rotations -II: Classification, *Finite Elements in Analysis and Design*, 24, 1997, pp.237-352.

[10] Gummadi, L. N. B and Palazotto, A. N., Large Strain Analysis of Beams and Arches undergoing Large Rotations, *Interantional Journal of non-linear Mechanics*, Vol.33, No.4, 1998, pp.615-645.

[11] Pai, P. F. and Palazotto, A. N., Nonlinear displacement-based finite-element analyses of composite shells– a new total Lagrangian formulation, *International Journal of Solids and Structures*, Vol. 32, 1995, pp.3047-3073.

[12] Greer, J. M. and Palazotto, A. N. Tire Contact using Two-Dimensional Finite Elements, Journal of Engineering Mechanics, Vol. 124, No. 3, March 1998, pp. 348-357.

[13] Gummadi, L. N. B and Palazotto, Total Lagrangian Approach to Non-linear Finite Element Approach to Nonlinear Finite Element Analysis of Cylindrical Shell Considering Large Rotations, *In 37th AIAA/ ASME/ ASCE/ AHS SDM Conference,*Vol. AIAA-96-1592, 1996, pp.2034-2043.

[14] Greer, J. M., Non-linear Finite Element Analysis of Composite Shells by Total Lagrangian Decomposition with Application to the Aircraft Tire, Ph.D. Dissertation AFIT/DS/ENY/96-1, The Air Force Institute of Technology, Graduate School of Engineering, Department of Aeronautics and Astronautics, 1996.

[15] Greer, J. M. and Palazotto, A. N., Non-linear Finite Element Analysis of Isotropic and Composite Shells by Total Lagrangian Decomposition Scheme, Mechanics of Composite Materials and Structures, Vol. 3, 1996, pp. 241-271.

REPORT DOCUMENTATION PAGE

Form Approved OMB No. 0704-0188

Public reporting burden for this collection of information is estimated to average 1 hour per response, including the time for reviewing instructions, searching existing data sources, gathering and maintaining the data needed, and completing and reviewing the collection of information. Send comments regarding this burden estimate or any other aspect of this collection of information, including suggestions for reducing this burden, to Washington Headquarters Services, Directorate for Information Operations and Reports, 1215 Jefferson Davis Highway, Suite 1204, Arlington, VA 22202-4302, and to the Office of Management and Budget, Paperwork Reduction Project (0704-0188), Washington, DC 20503.

1. AGENCY USE ONLY *(Leave blank)*	2. REPORT DATE	3. REPORT TYPE AND DATES COVERED
	September 1998	Interim Report

4. TITLE AND SUBTITLE
The Analysis of Inflatable Antennas Using A Corotational Finite Element Analysis

5. FUNDING NUMBERS

6. AUTHOR(S)
A. N. Palazotto, J. O. Choi

7. PERFORMING ORGANIZATION NAME(S) AND ADDRESS(ES)
Air Force Institute of Technology, Department of Aeronautical and Astronautical Engineering
2950 P Street, Bldg 640
Wright-Patterson AFB, Ohio 45433-7765

8. PERFORMING ORGANIZATION REPORT NUMBER
AFIT/ENY/TR-98-04

9. SPONSORING/MONITORING AGENCY NAME(S) AND ADDRESS(ES)
AFIT/ENY
2950 P Street, Bldg 640
WPAFB OH 45433-7765

10. SPONSORING/MONITORING AGENCY REPORT NUMBER

11. SUPPLEMENTARY NOTES

12a. DISTRIBUTION AVAILABILITY STATEMENT
Approved for public release.

12b. DISTRIBUTION CODE

13. ABSTRACT *(Maximum 200 words)*

The Jaumann stress-strain approach has been used to evaluate a nonlinear structural response to a shell like geometry. The method employs a finite element solution incorporating the Jaumann stress-strain relationships based on large displacement and large rotation using a corotational technique. It is possible to evaluate the effects of direct and shear stresses within a laminated structure. Results show that the need for a correct thorough evaluation of the stresses of the shell is required as the shell thickness increases relative to the resulting geometry. In a predominately membrane resistant structure, the three types of theories, Eulerian, Jaumann and Lagrangian show close comparison.

DTIC

14. SUBJECT TERMS	15. NUMBER OF PAGES
	67
	16. PRICE CODE

17. SECURITY CLASSIFICATION OF REPORT	18. SECURITY CLASSIFICATION OF THIS PAGE	19. SECURITY CLASSIFICATION OF ABSTRACT	20. LIMITATION OF ABSTRACT
Unclassified	Unclassified	Unclassified	

Standard Form 298 (Rev. 2-89) (EG)
Prescribed by ANSI Std. 239.18
Designed using Perform Pro, WHS/DIOR, Oct 94